CHASER: A global chemical model of the troposphere 1. Model description

Kengo Sudo,[1] Masaaki Takahashi,[1] Jun-ichi Kurokawa,[2] and Hajime Akimoto[3]

Received 10 July 2001; revised 22 January 2002; accepted 8 February 2002; published 13 September 2002.

[1] We present a new global three-dimensional chemical model for the troposphere, named chemical atmospheric general circulation model (AGCM) for study of atmospheric environment and radiative forcing (CHASER). This model, developed in the framework of the Center for Climate System Research/National Institute for Environment Studies (CCSR/NIES) AGCM, is aimed to study tropospheric photochemistry and its influences on climate. The chemical component of the model simulates the O_3-HO_x-NO_x-CH_4-CO photochemical system and oxidation of nonmethane hydrocarbons through 88 chemical and 25 photolytic reactions with 47 chemical species in its present configuration. The model includes emission sources, dry and wet deposition, as well as chemical transformations. Meteorological processes such as transport due to advection, convection, and other subgrid-scale mixing are simulated "on-line" by the dynamical component of the CCSR/NIES AGCM. A detailed evaluation of the model results is presented in a companion paper [*Sudo et al.*, 2002]. An evaluation of the transport scheme adopted in the model suggests that the model is capable of simulating transport associated with convection and boundary layer mixing as well as large-scale advection. The model capability to simulate dry and wet deposition was also evaluated by conducting a simulation of atmospheric lead. The simulated lead distributions are consistent with those observed at the surface, showing the validity of the deposition parameterization adopted in the model. *INDEX TERMS:* 0365 Atmospheric Composition and Structure: Troposphere—composition and chemistry; 0368 Atmospheric Composition and Structure: Troposphere—constituent transport and chemistry; 3337 Meteorology and Atmospheric Dynamics: Numerical modeling and data assimilation; 3319 Meteorology and Atmospheric Dynamics: General circulation

Citation: Sudo, K., M. Takahashi, J. Kurokawa, and H. Akimoto, CHASER: A global chemical model of the troposphere, 1. Model description, *J. Geophys. Res.*, *107*(D17), 4339, doi:10.1029/2001JD001113, 2002.

1. Introduction

[2] The direct and indirect impact of human activities on the atmospheric environment and climate is one of the biggest concerns in recent atmospheric science. The chemical composition of the atmosphere has been changed by not only increase in anthropogenic emission, but also changes in land use. In addition to well-mixed gases as carbon dioxide (CO_2) and methane (CH_4), reactive species such as ozone (O_3) and its precursors (carbon monoxide CO, nitrogen oxides NO_x, nonmethane hydrocarbons NMHCs, etc.) are on the increase [e.g., *Crutzen and Zimmermann*, 1991]. Ozone, a greenhouse gas as well as CO_2 and CH_4, is the most important chemical species for tropospheric photochemistry to activate chemical reactions and control the life time of other chemical species (oxidation capacity) through formation of hydroxy radical (OH). The impact of these changes in the atmospheric composition on the atmospheric environment and climate is at the global scale. Therefore, global investigation of the behavior of individual chemical species and each process is needed.

[3] Global chemical models can easily incorporate and reflect one's suggestions in terms of global effect. Additionally, comparisons between model results and observations show us rightness of the present knowledge about atmospheric chemistry or sometimes suggest other possibilities.

[4] There have been various modeling studies of the global tropospheric ozone, chemistry, and transport up to the present [*Levy et al.*, 1985; *Müller and Brasseur*, 1995; *Roelofs and Lelieveld*, 1995; *Berntsen and Isaksen*, 1997; *Brasseur et al.*, 1998; *Hauglustaine et al.*, 1998; *Wang et al.*, 1998a, 1998b; *Lawrence et al.*, 1999]. *Roelofs and Lelieveld* [1995] and *Lawrence et al.* [1999] simulated O_3-HO_x-NO-CO-CH_4 chemistry in the troposphere. *Müller and Brasseur* [1995], *Brasseur et al.* [1998], *Hauglustaine et al.* [1998], and *Wang et al.* [1998a, 1998b] simulated global tropospheric chemistry including NMHCs. *Wang et al.* [1998c] and *Roelofs and Lelieveld* [2000] reported the influence of NMHCs on tropospheric chemistry. In addition

[1]Center for Climate System Research, University of Tokyo, Tokyo, Japan.
[2]Systems Department, Environmental Systems Business Division, Fujitsu FIP Corporation, Tokyo, Japan.
[3]Institute for Global Change Research, Kanagawa, Japan.

0148-0227/02/2001JD001113$09.00

to tropospheric chemistry of ozone, global radiative forcing by the tropospheric ozone increase is also a great concern. Some studies investigated the radiative forcing of tropospheric ozone using simulated global ozone concentrations [*Roelofs et al.*, 1997; *Haywood et al.*, 1998; *Roelofs and Lelieveld*, 2000; *Mickley et al.*, 2001]. They concluded that the radiative forcing by the tropospheric ozone change is as important as that of other greenhouse gases especially in the Northern Hemisphere.

[5] In this paper, we introduce a new global chemical model of the troposphere named CHASER. This model is based on the Center for Climate System Research (CCSR), University of Tokyo/National Institute for Environmental Studies (NIES) AGCM, which has been developed at the CCSR and the NIES. The CCSR/NIES AGCM has been also used for an on-line global simulation of stratospheric chemistry and dynamics [*Takigawa et al.*, 1999], and for a global simulation of the aerosol distribution and optical thickness of various origins [*Takemura et al.*, 2000]. The principal objective of CHASER is to study the global distributions and budgets of ozone and its precursors. Additionally, CHASER can be used to assess the global impact of changes in the atmospheric composition on climate. CHASER has been already employed in a simulation study of tropospheric ozone changes during the 1997–1998 El Niño event [*Sudo and Takahashi*, 2001].

[6] CHASER includes transport, chemistry, deposition, and radiation components. Calculated ozone concentration is used for the radiation and photolysis rate (J-value) calculation. We describe a model overview in section 2. Description and evaluation of the transport component are given in section 3. We introduce the chemistry component and emissions used in this study in section 4 and section 5, respectively. In section 6, the deposition processes in CHASER are described and evaluated. A detailed evaluation of the model results of ozone and related chemical species is presented by *Sudo et al.* [2002].

2. Model Overview

[7] The CHASER model is based on the CCSR/NIES AGCM. Basic features of the CCSR/NIES AGCM have been described by *Numaguti* [1993]. The newly implemented physical processes were presented by *Numaguti et al.* [1995]. This AGCM adopts a radiation scheme based on the k-distribution and the two-stream discrete ordinate method [*Nakajima and Tanaka*, 1986]. A detailed description of the radiation scheme adopted in the AGCM is given by *Nakajima et al.* [1995]. The prognostic Arakawa-Schubert scheme is employed to simulate cumulus convection [cf. *Numaguti et al.*, 1995] (see the description by *Numaguti* [1999] for further details of the hydrological processes in the model). The level 2 scheme of turbulence closure by *Mellor and Yamada* [1974] is used for the estimation of the vertical diffusion coefficient. The orographic gravy wave momentum deposition in the AGCM is parameterized following *McFarlane* [1987]. The AGCM generally reproduces the climatology of meteorological fields. In climatological simulations, CHASER uses climatological data of sea surface temperature (SST) as an input to the AGCM. In simulations of a specific time period, analyzed data of wind velocities, temperature, and specific humidity from the European Center for Medium-Range Weather Forecasts (ECMWF) are used as a constraint in addition to SST data of a corresponding year, because it may be difficult to validate just climatological output from the model with observations in a certain period.

[8] In CHASER, dynamical processes such as tracer transport, vertical diffusion, surface emissions, and deposition are simulated in the flow of the AGCM calculation. The chemistry component of CHASER calculates chemical transformations using variables of the AGCM (e.g., temperature, pressure, humidity). In the radiation component, radiative transfer and photolysis rates are calculated by using the concentrations of chemical species calculated in the chemistry component. The dynamical and physical components of CHASER are evaluated with a time step of 30 min. We have chosen a chemistry time step of 10 min. In this study, we adopted a horizontal spectral resolution of T21 (approximately, 5.6° longitude × 5.6° latitude) with 32 layers in the vertical from the surface up to about 3 hPa (about 40 km) altitude. CHASER uses the σ coordinate system in the vertical. The 32 layers are centered approximately at 995, 980, 950, 900, 830, 745, 657, 576, 501, 436, 380, 331, 288, 250, 218, 190, 165, 144, 125, 109, 95, 82, 72, 62, 54, 47, 40, 34, 27, 19, 11, and 3 hPa, resulting in a vertical resolution of 1 km in the free troposphere and much of the lower stratosphere for an accurate representation of vertical transport such as the stratosphere-troposphere exchange (STE).

[9] The present version of CHASER calculates the concentrations of 44 chemical species from the surface up to about 20 km altitude. The concentrations of O_3, NO_x, N_2O_5, and HNO_3 in the stratosphere (above 20 km altitude) are prescribed using monthly averaged output data from a three-dimensional stratospheric chemical model [*Takigawa et al.*, 1999]. For the O_3 distribution (>20 km), the data of *Takigawa et al.* [1999] were scaled by using zonal mean satellite data from the Halogen Occultation Experiment project (HALOE) [*Russel et al.*, 1993; *Randel*, 1998], since the latest version of the stratospheric chemical model [*Takigawa et al.*, 1999] tends to slightly overestimate the O_3 concentrations in the tropical lower stratosphere. Concentrations in the stratosphere (>20km) in the model are reset to those data at each time step.

[10] Information about the CHASER model can also be obtained via http://atmos.ccsr.u-tokyo.ac.jp/~kengo/chaser.

3. Transport

[11] Transport is one of the most important processes to simulate the atmospheric photochemistry. Emitted or chemically produced species undergo advection by large-scale wind field and subgrid vertical transport by diffusion and moist convection. In CHASER, advective transport is simulated by a 4th order flux-form advection scheme of the monotonic van Leer [*van Leer*, 1977], except for the vicinity of the poles. For a simulation of advection around the poles, the flux-form semi-Lagrangian scheme of *Lin and Rood* [1996] is used. Vertical transport associated with moist convection (updrafts and downdrafts) is simulated by the cumulus convection scheme (the prognostic Ara-

kawa-Schubert scheme). In the boundary layer, equations of vertical diffusion and surface emission and deposition fluxes are solved implicitly.

[12] It is necessary to validate the model capability for simulations of transport. For this purpose, we have conducted a simple simulation of the distribution of atmospheric radon (^{222}Rn). Radon is emitted from the Earth's surface (mainly from land surface) and decays radioactively with a lifetime of 5.5 days. Surface emission of radon considered here is generally based on the study of *Jacob et al.* [1997], in which radon emission from land surface is set 1.0 atoms cm^{-2} s^{-1} uniformally. Some simulation studies based on this radon emission scenario, however, show an underestimation of the simulated radon concentrations at Mauna Loa by a factor of 2–3 compared to observations, with showing relatively good agreement of simulations with observations at other sites [*Jacob et al.*, 1997; *Brasseur et al.*, 1998]. Although there is a possibility that an insufficient transport in the simulations causes this discrepancy on one side, it can be attributed to a higher emission rate of radon in eastern Asia as suggested by *Mahowald et al.* [1997]. To take this into account, emission rate in eastern Asia (10°S–55°N, 100°E–160°E) is tentatively increased by a factor of 2 in this simulation.

[13] Figure 1 shows the simulated radon distributions for June–July–August (JJA). As can be seen in zonal mean distribution (upper panel), radon is vertically transported from the surface up to the tropopause height associated with convective activities in the Northern Hemisphere. Horizontal distribution of radon in the upper troposphere can be seen in the lower panel of Figure 1. An outstanding high concentration over eastern Asia is due to the doubled emission rate in this region. Transport of radon from northern America and Africa to over the Atlantic is seen. Moreover, long range transport of radon from eastern Asia appears to reach the eastern Pacific region including western America. Figure 2 compares the simulated and the observed radon vertical profiles in western America (California) for June and JJA conditions. The model appears to reproduce the observed radon vertical distribution in the middle-upper troposphere well. The radon maximum seen at 8–10 km altitude is much associated with long range transport from eastern Asia, according to *Stockwell et al.* [1998]. This feature is clearly seen in Figure 3 showing the cross-sectional distribution of calculated radon over 36°N for June. It can be seen that the radon distribution in the middle-upper troposphere is largely affected by transport from eastern Asia through much of the eastern Pacific and western America. In Figure 2, radon concentration is slightly underestimated by the model in 1–3 km altitudes, whereas is overestimated at the surface. This may indicate an insufficient mixing between the planetary boundary layer and the lower troposphere. Figure 4 shows a comparison of calculated and observed seasonal variations of surface radon at several sites. The model appears to reproduce observed radon seasonal cycle well. Both the concentration and the time variability of calculated surface radon are generally high in wintertime when vertical transport of emitted radon is not efficient due to low convective activity. The seasonal cycle of spring-maximum at Mauna Loa is also well reproduced with the doubled radon emission in eastern Asia.

4. Chemistry

[14] The chemistry component of CHASER includes 34 tracers (transported) and 16 nontracers (radical species and members of family tracers). Table 1 shows chemical species considered in CHASER. Ozone and nitrogen oxides (NO + NO_2 + NO_3) are transported as families (O_x and NO_x, respectively). The concentrations of nitrogen (N_2), oxygen (O_2), and water vapor (H_2O) are determined from the AGCM calculation. In this study, CH_4 is not considered as a tracer because of its long chemical lifetime (8–11 years). In the model, CH_4 concentration is assumed to be 1.77 ppmv and 1.68 ppmv in the northern and the southern hemisphere, respectively.

[15] The present version of CHASER includes 25 photolytic reactions and 88 chemical reactions (Tables 2 and 3). It considers NMHCs oxidation as well as the O_x-HO_x-NO_x-CH_4-CO chemical system. Oxidations of ethane (C_2H_6), propane (C_3H_8), ethene (C_2H_4), propene (C_3H_6), isoprene (C_5H_8), and terpenes ($C_{10}H_{16}$, etc.) are included explicitly. Degradation of other NMHCs is represented by the oxidation of a lumped species named other nonmethane volatile organic compounds (ONMV) as in the IMAGES model [*Müller and Brasseur*, 1995] and the MOZART model [*Brasseur et al.*, 1998]. We adopted a condensed isoprene oxidation scheme of *Pöschl et al.* [2000] which is based on the Master Chemical Mechanism (MCM, Version 2.0) [*Jenkin et al.*, 1997]. Terpenes oxidation is largely based on the study of *Brasseur et al.* [1998] (the MOZART model). Acetone is believed to be an important source of HO_x in the upper troposphere and affect the background PAN formation in spite of its low photochemical activity. Acetone chemistry and propane oxidation are, therefore, included in this study, based on the MCM, Version 2.0. Heterogeneous reactions on aerosols may reduce the levels of NO_x, HO_x, and some RO_2 radicals [*Dentener and Crutzen*, 1993; *Jaeglé et al.*, 1999; *Jacob*, 2000]. However, heterogeneous reactions on aerosols are not considered in this study. They are being implemented in the next version of CHASER.

[16] Reaction rates for the reactions listed in Tables 2 and 3 are mainly taken from *DeMore et al.* [1997] and *Atkinson et al.* [2000] and *Sander et al.* [2000] for updated reactions. The quantum yield for $O(^1D)$ production in ozone photolysis (J1) is based on the work of *Talukdar et al.* [1998]. The photolysis rates (J-values) are calculated on-line by using temperature and radiation fluxes computed in the radiation component of CHASER. The radiation scheme adopted in CHASER (based on the CCSR/NIES AGCM) considers the absorption and scattering by gases, aerosols and clouds, and the effect of surface albedo. In the CCSR/NIES AGCM, the original wavelength resolution for the radiation calculation is relatively coarse in the ultraviolet and the visible wavelength regions as in general AGCMs. Therefore, the wavelength resolution in these wavelength regions has been improved for the photochemistry in CHASER. In addition, representative absorption cross sections and quantum yields for individual spectral bins are evaluated depending on the optical

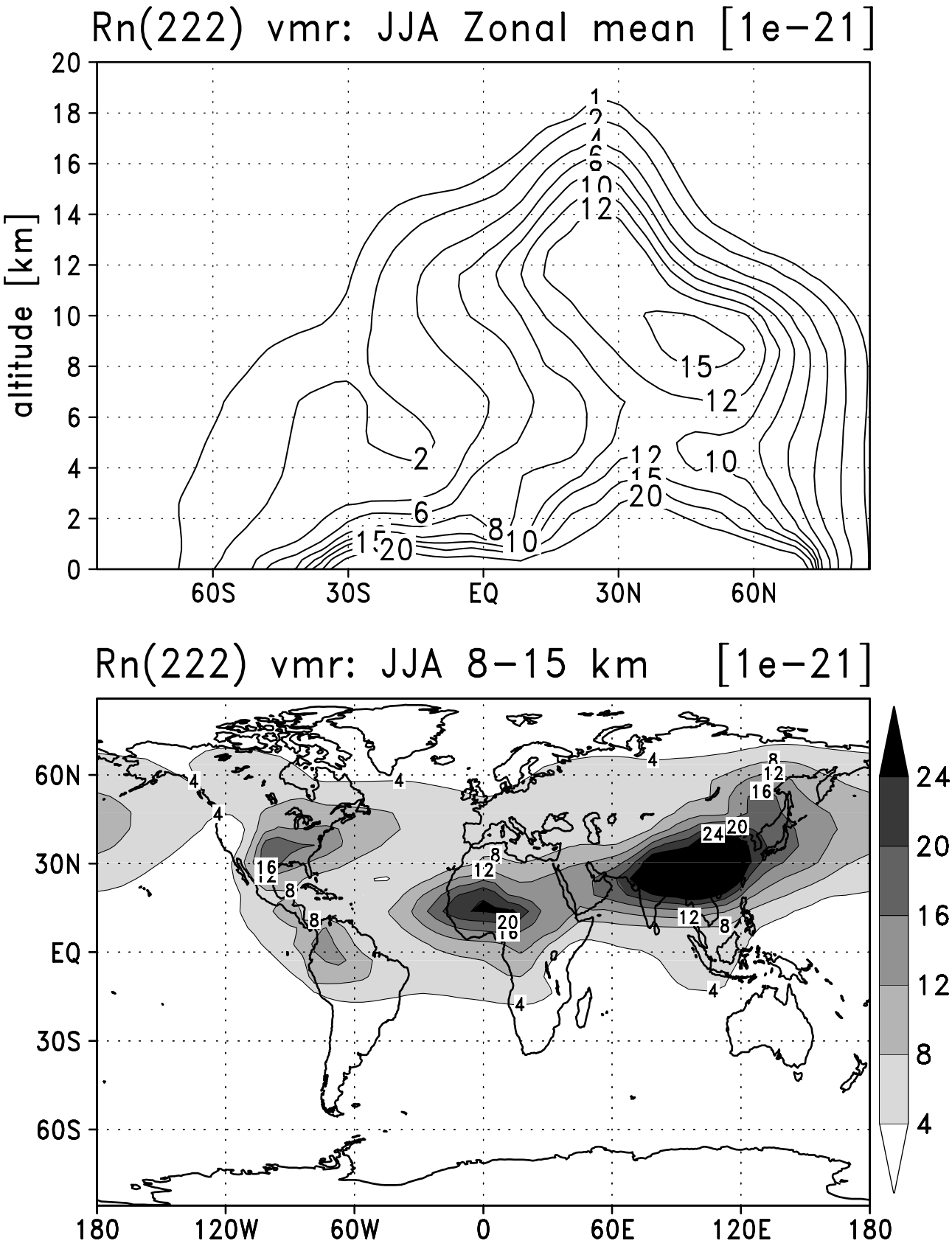

Figure 1. Calculated distribution (volume mixing ratio) of radon for June–July–August. The distribution in the upper panel is zonally averaged, and averaged over 8–15 km altitude for the lower panel.

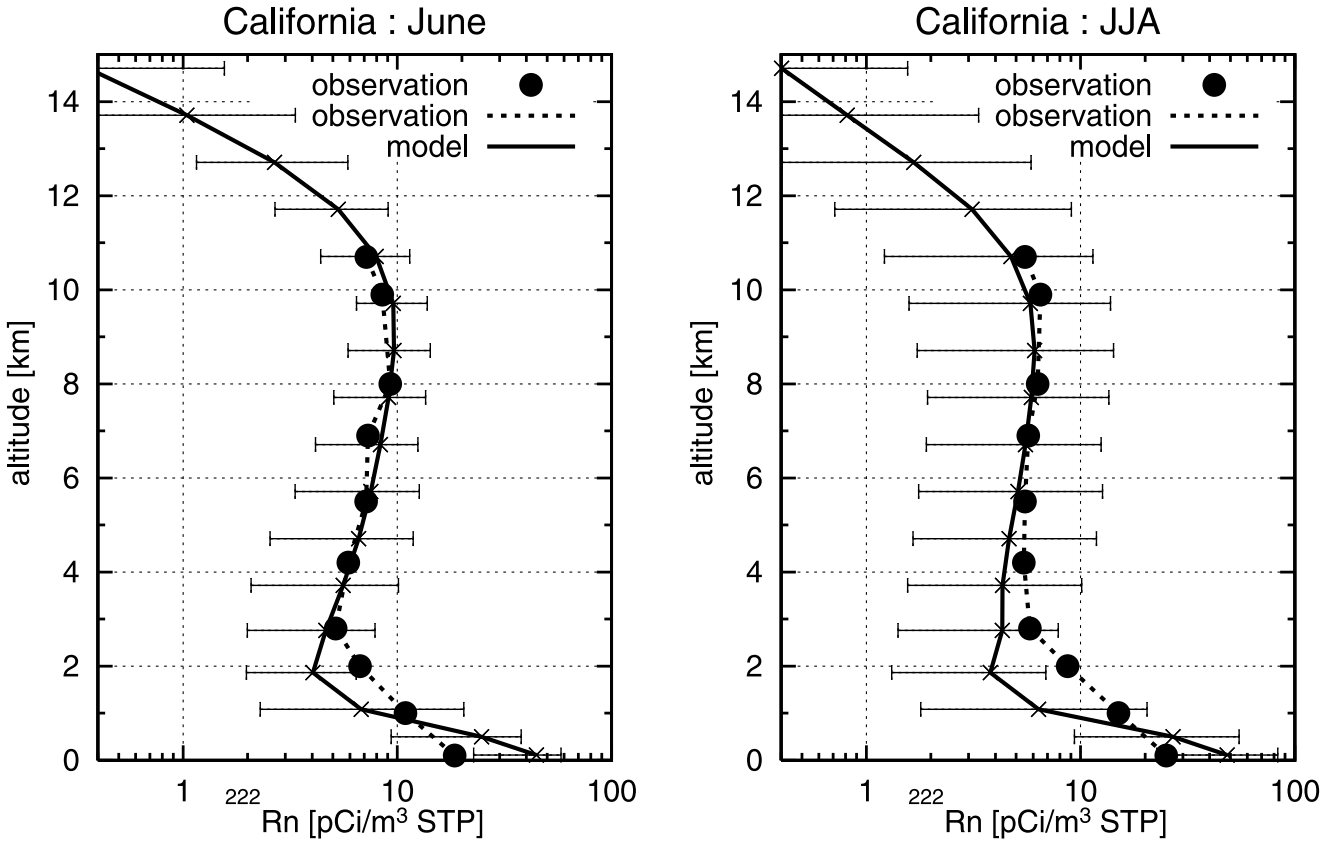

Figure 2. Calculated (solid lines) and observed (solid circles and dashed lines) radon vertical profiles in California (37.4°N, 122°W). The values are June average (left panel) and June–July–August average (right panel). Error bars with calculated profiles show the range. Observation is from *Kritz et al.* [1998].

thickness computed in the radiation component, in a way similar to that of *Landgraf and Crutzen* [1998]. The photolysis rate for the $O_3 \rightarrow O(^1D)$ reaction calculated for January and July can be seen in Figure 5.

[17] CHASER uses an Euler Backward Iterative (EBI) method to solve the chemical reaction system. The method is largely based on the work of *Hertel et al.* [1993] which increases the efficiency of the iteration process by using

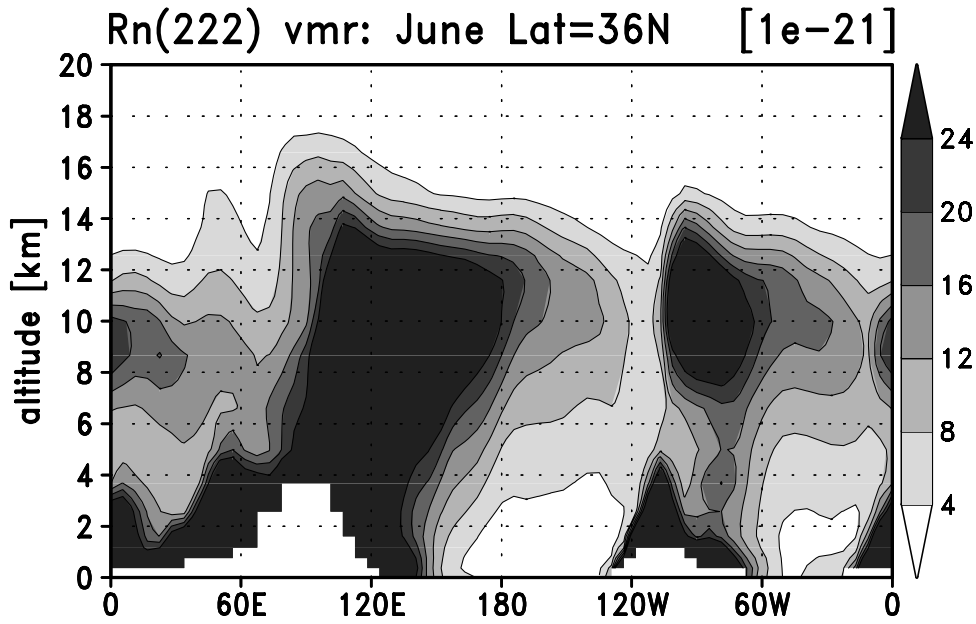

Figure 3. Calculated distribution (volume mixing ratio) of radon in June for 36°N.

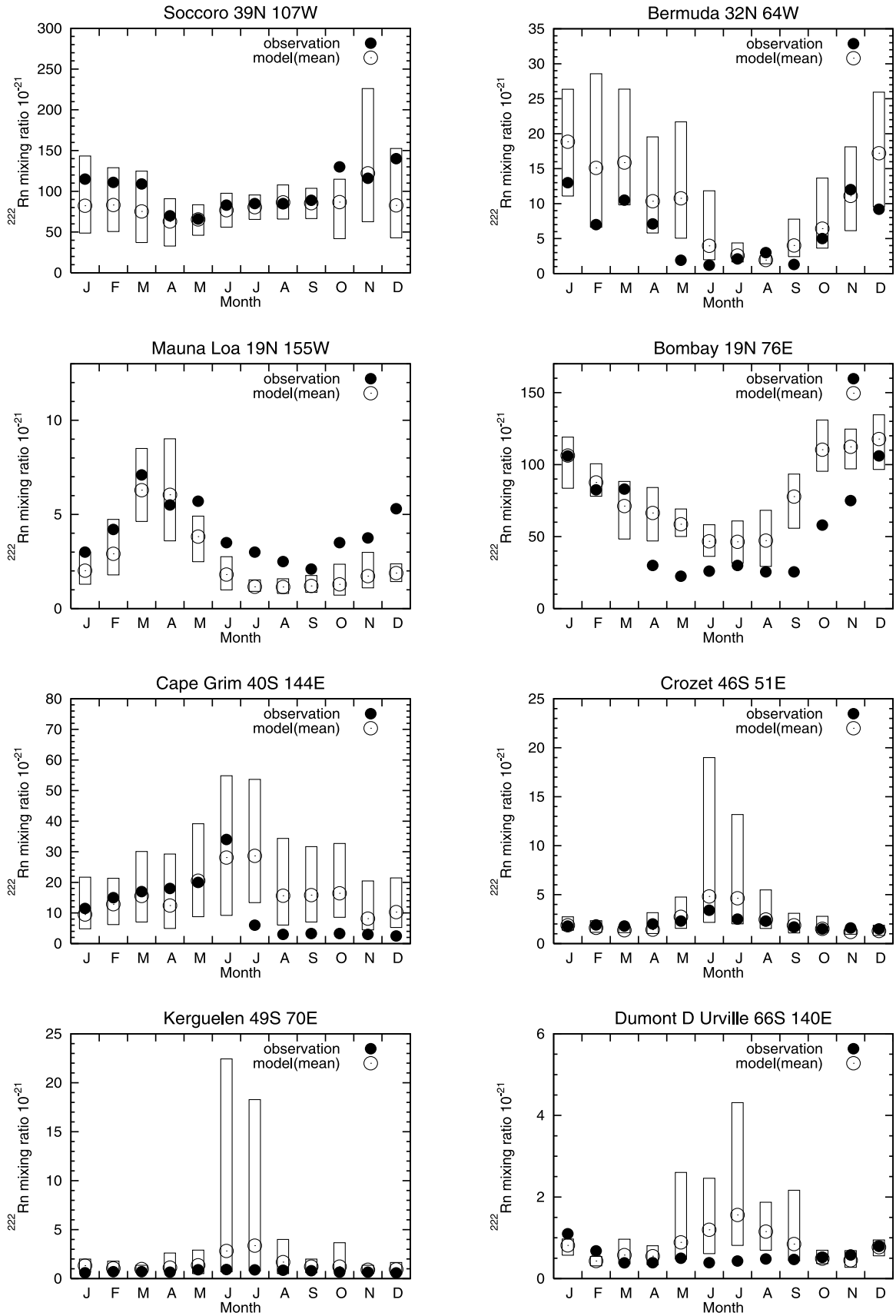

Figure 4. Calculated (open circles) and observed (filled circles) surface radon (^{222}Rn) seasonal variations. Boxes show the range of calculated values.

Table 1. Chemical Species Considered in CHASER

No.	Name	Family	Description
Tracers			
01	O_x	$O_3 + O(^1D)$	O_x family
02	NO_x	$NO + NO_2 + NO_3$	NO_x family
03	N_2O_5	single	nitrogen pentoxide
04	HNO_3	single	nitric acid
05	HNO_4	single	peroxynitric acid
06	H_2O_2	single	hydrogen peroxide
07	CO	single	carbon monoxide
08	C_2H_6	single	ethane
09	C_3H_8	single	propane
10	C_2H_4	single	ethene
11	C_3H_6	single	propene
12	ONMV	single	other NMVOCs[a]
13	C_5H_8	single	isoprene
14	$C_{10}H_{16}$	single	terpenes
15	CH_3COCH_3	single	acetone
16	CH_2O	single	formaldehyde
17	CH_3CHO	single	acetaldehyde
18	NALD	single	nitrooxy acetaldehyde
19	MGLY	single	methylglyoxal and other C_3 aldehydes
20	HACET	single	hydroxyacetone and C_3 ketones
21	MACR	single	methacrolein, methylvinylketone C_4 carbonyls
22	PAN	single	peroxyacetyl nitrate
23	MPAN	single	higher peroxyacetyl nitrates
24	ISON	single	isoprene nitrates
25	CH_3OOH	single	methyl hydro-peroxide
26	C_2H_5OOH	single	ethyl hydro-peroxide
27	C_3H_7OOH	single	propyl hydro-peroxide
28	HOROOH	single	peroxides from C_2H_4 and C_3H_6
29	ISOOH	single	hydro-peroxides from $ISO_2 + HO_2$
30	CH_3COOOH	single	paracetic acid
31	MACROOH	single	hydro-peroxides from $MACRO_2 + HO_2$
32	O_x(S)	O_3(S) + $O(^1D)$(S)	O_x family from the stratosphere
33	^{222}Rn	single	radon(222)
34	^{210}Pb	single	lead(210)
Nontracers[b]			
01	OH		hydroxyl radical
02	HO2		hydroperoxyl radical
03	CH_3O2		methyl peroxy radical
04	C_2H_5O2		ethyl peroxy radical
05	C_3H_7O2		propyl peroxy radical
06	CH_3COO_2		peroxy acetyl radical
07	$CH_3COCH_2O_2$		acetylmethyl peroxy radical
08	$HOC_2H_4O_2$		hydroxy ethyl peroxy radical
09	$HOC_3H_6O_2$		hydroxy propyl peroxy radical
10	ISO_2		peroxy radicals from C_5H_8 + OH
11	$MACRO_2$		peroxy radicals from MACR + OH

[a]Nonmethane volatile organic compounds.
[b]Not including member species of family tracers.

analytical solutions for strongly coupled species (e.g., OH-HO_2). The chemical equations are solved with a time step of 10 min in this study. Configurations of the chemical scheme such as a choice of species, reactions, and reaction rates are automatically processed by the preprocessor to set up the model through input files. Therefore, the chemical reaction system as listed in Tables 2 and 3 can be easily changed by a user.

5. Emissions

[18] Surface emissions are considered for CO, NO_x and NMHCs in the model (Table 4). Anthropogenic emissions associated with industry (e.g., fossil fuel combustion) and car traffic are based on the Emission Database for Global Atmospheric Research (EDGAR) Version 2.0 [*Olivier et al.*, 1996]. NMHCs emissions from ocean are taken from *Müller* [1992] as in the MOZART model. The geographical distribution of biomass burning is taken from *Hao and Liu* [1994]. The emission rates of NMHCs by biomass burning were scaled to the values adopted in the MOZART model [*Brasseur et al.*, 1998]. The active fire (Hot Spot) data derived from Advanced Very High Resolution Radiometer (AVHRR) and Along Track Scanning Radiometer (ATSR) [*Arino et al.*, 1999] are used as a scaling factor to simulate the seasonal variation of biomass burning emissions. In this study, we estimated the timing of biomass burning emissions, using the hot spot data for 1999 derived from ATSR. We assumed that individual daily hot spots in a model grid cause emissions which decline in a timescale of 20 days in that grid. The temporal resolution for biomass burning emissions is 10 days in this study. Simulated biomass burning emissions in South America have peaks in late August and September (e.g., CO emission, Figure 6). In

Table 2. Photolytic Reactions Included in CHASER

No.	Reaction	Ref.
J1)	$O_3 + h\nu \rightarrow O(^1D) + O_2$	1, 2
J2)	$H_2O_2 + h\nu \rightarrow 2\ OH$	1
J3)	$NO_2 + h\nu \rightarrow NO + O_3$	1
J4)	$NO_3 + h\nu \rightarrow 0.1\ NO + 0.9\ NO_2 + 0.9\ O_3$	1
J5)	$N_2O_5 + h\nu \rightarrow NO_2 + NO_3$	1
J6)	$HNO_3 + h\nu \rightarrow NO_2 + OH$	1
J7)	$HNO_4 + h\nu \rightarrow NO_2 + HO_2$	1
J8)	$PAN + h\nu \rightarrow CH_3COO_2 + NO_2$	1
J9)	$CH_3OOH + h\nu \rightarrow CH_2O + OH + HO_2$	1
J10)	$C_2H_5OOH + h\nu \rightarrow CH_3CHO + OH + HO_2$	1
J11)	$C_3H_7OOH + h\nu \rightarrow 0.24\ C_2H_5O_2 + 0.09\ CH_3CHO + 0.18\ CO + 0.7\ CH_3COCH_3 + OH + HO_2$	1
J12)	$CH_3COCH_3 + h\nu \rightarrow CH_3COO_2 + CH_3O_2$	3
J13)	$HOROOH + h\nu \rightarrow 0.5\ CH_3CHO + 1.5\ CH_2O + HO_2 + H_2O$	1
J14)	$CH_3COOOH + h\nu \rightarrow CH_3O_2 + CO_2 + OH$	4
J15)	$CH_2O + h\nu \rightarrow CO + 2\ HO_2$	1
J16)	$CH_2O + h\nu \rightarrow CO + 2\ H_2$	1
J17)	$CH_3CHO + h\nu \rightarrow CH_3O_2 + CO + HO_2$	5
J18)	$ISOOH + h\nu \rightarrow MACR + CH_2O + OH + HO_2$	1
J19)	$ISON + h\nu \rightarrow NO_2 + MACR + CH_2O + HO_2$	1, 6, 7
J20)	$MACR + h\nu \rightarrow CH_3COO_2 + CH_2O + CO + HO_2$	6, 7, 8
J21)	$MPAN + h\nu \rightarrow MACRO_2 + NO_2$	1
J22)	$MACROOH + h\nu \rightarrow OH + 0.5\ HACET + 0.5\ CO + 0.5\ MGLY + 0.5\ CH_2O + HO_2$	1
J23)	$HACET + h\nu \rightarrow CH_3COO_2 + CH_2O + HO_2$	1, 6
J24)	$MGLY + h\nu \rightarrow CH_3COO_2 + CO + HO_2$	5, 6, 7
J25)	$NALD + h\nu \rightarrow CH_2O + CO + NO_2 + HO_2$	5

References: 1, *DeMore et al.* [1997]; 2, *Talukdar et al.* [1998]; 3, *Gierczak et al.* [1998]; 4, *Müller and Brasseur* [1995]; 5, *Atkinson et al.* [1999]. 6, *Jenkin et al.* [1997]; 7, *Pöschl et al.* [2000]; 8, *Carter* [1990].

Table 3. Chemical Reactions Included in CHASER

No.	Reaction	Rate	Ref.
K1)	$O(^1D) + O_2 \rightarrow O_3 + O_2$	$k_1 = 3.20\text{E-}11\ \exp(70/T)$	1
K2)	$O(^1D) + N_2 \rightarrow O_3 + N_2$	$k_2 = 1.80\text{E-}11\ \exp(110/T)$	1
K3)	$O(^1D) + H_2O \rightarrow 2\ OH$	$k_3 = 2.20\text{E-}10$	1
K4)	$O_3 + OH \rightarrow HO_2 + O_2$	$k_4 = 1.50\text{E-}12\ \exp(-880/T)$	1
K5)	$O_3 + HO_2 \rightarrow OH + 2\ O_2$	$k_5 = 2.00\text{E-}14\ \exp(-680/T)$	1
K6)	$O_3 + NO \rightarrow NO_2 + O_2$	$k_6 = 3.00\text{E-}12\ \exp(-1500/T)$	1
K7)	$O_3 + NO_2 \rightarrow NO_3 + O_2$	$k_7 = 1.20\text{E-}13\ \exp(-2450/T)$	1
K8)	$OH + HO_2 \rightarrow H_2O + O_2$	$k_8 = 4.80\text{E-}11\ \exp(250/T)$	1
K9)	$OH + H_2O_2 \rightarrow H_2O + HO_2$	$k_9 = 2.90\text{E-}12\ \exp(-160/T)$	1
K10)	$HO_2 + NO \rightarrow NO_2 + OH$	$k_{10} = 3.50\text{E-}12\ \exp(250/T)$	1
K11)	$HO_2 + HO_2 \rightarrow H_2O_2 + O_2$	$(k_a + k_b\ [M])\ k_c$ $k_a = 2.30\text{E-}13\ \exp(600/T)$ $k_b = 1.70\text{E-}33\ \exp(1000/T)$ $k_c = 1 + 1.40\text{E-}21\ [H_2O]\ \exp(2200/T)$	1
K12)	$OH + NO_2 + M \rightarrow HNO_3 + M$	$k_0 = 2.40\text{E-}30\ (300/T)^{3.1}$ $k_\infty = 1.70\text{E-}11\ (300/T)^{2.1}$ $F_c = 0.6$	1
K13)	$OH + HNO_3 \rightarrow NO_3 + H_2O$	$k_{13} = k_a + k_b\ [M]/(1 + k_b\ [M]/k_c)$ $k_a = 2.40\text{E-}14\ \exp(460/T)$ $k_b = 6.50\text{E-}34\ \exp(1335/T)$ $k_c = 2.70\text{E-}17\ \exp(2199/T)$	1
K14)	$NO_2 + NO_3 + M \rightarrow N_2O_5 + M$	$k_0 = 2.00\text{E-}30\ (300/T)^{4.4}$ $k_\infty = 1.40\text{E-}12\ (300/T)^{0.7}$ $F_c = 0.6$	1
K15)	$N_2O_5 + M \rightarrow NO_2 + NO_3 + M$	$k_{15} = k_{14}/(2.70\text{E-}27\ \exp(11000/T))$	1
K16)	$N_2O_5 + H_2O \rightarrow 2\ HNO_3$	$k_{16} = 2.10\text{E-}21$	1
K17)	$NO_3 + NO \rightarrow 2\ NO_2$	$k_{17} = 1.50\text{E-}11\ \exp(170/T)$	1
K18)	$NO_2 + HO_2 + M \rightarrow HNO_4 + M$	$k_0 = 1.80\text{E-}31\ (300/T)^{3.2}$ $k_\infty = 4.70\text{E-}12\ (300/T)^{1.4}$ $F_c = 0.6$	1
K19)	$HNO_4 + M \rightarrow NO_2 + HO_2 + M$	$k_{19} = k_{18}/(2.10\text{E-}27\ \exp(10900/T))$	1
K20)	$HNO_4 + OH \rightarrow NO_2 + H_2O + O_2$	$k_{20} = 1.30\text{E-}12\ \exp(380/T)$	
	CH_4 Oxidation		
K21)	$CH_4 + OH \rightarrow CH_3O_2 + H_2O$	$k_{21} = 2.45\text{E-}12\ \exp(-1775/T)$	1
K22)	$CH_4 + O(^1D) \rightarrow CH_3O_2 + OH$	$k_{22} = 1.50\text{E-}10$	2
K23)	$CH_3O_2 + NO \rightarrow CH_2O + NO_2 + HO_2$	$k_{23} = 3.00\text{E-}12\ \exp(280/T)$	1
K24)	$CH_3O_2 + CH_3O_2 \rightarrow 1.8\ CH_2O + 0.6\ HO_2$	$k_{24} = 2.50\text{E-}13\ \exp(190/T)$	1
K25)	$CH_3O_2 + HO_2 \rightarrow CH_3OOH + O_2$	$k_{25} = 3.80\text{E-}13\ \exp(800/T)$	1

Table 3. (continued)

No.	Reaction	Rate	Ref.
K26)	$CH_3OOH + OH \rightarrow 0.7\ CH_3O_2 + 0.3\ CH_2O + 0.3\ OH + H_2O$	$k_{26} = 3.80E\text{-}12\ \exp(200/T)$	1
K27)	$CH_2O + OH \rightarrow CO + HO_2 + H_2O$	$k_{27} = 1.00E\text{-}11$	1
K28)	$CH_2O + NO_3 \rightarrow HNO_3 + CO + HO_2$	$k_{28} = 6.00E\text{-}13\ \exp(-2058/T)$	3
K29)	$CO + OH \rightarrow CO_2 + HO_2$	$k_{29} = 1.50E\text{-}13\ (1 + 0.6\ P_{atm})$	1
	C_2H_6 and C_3H_8 Oxidation		
K30)	$C_2H_6 + OH \rightarrow C_2H_5O_2 + H_2O$	$k_{30} = 8.70E\text{-}12\ \exp(-1070/T)$	1
K31)	$C_2H_5O_2 + NO \rightarrow CH_3CHO + NO_2 + HO_2$	$k_{31} = 2.60E\text{-}12\ \exp(365/T)$	1
K32)	$C_2H_5O_2 + HO_2 \rightarrow C_2H_5OOH + O_2$	$k_{32} = 7.50E\text{-}13\ \exp(700/T)$	1
K33)	$C_2H_5O_2 + CH_3O_2 \rightarrow 0.8\ CH_3CHO + 0.6\ HO_2$	$k_{33} = 3.10E\text{-}13$	4
K34)	$C_2H_5OOH + OH \rightarrow 0.286\ C_2H_5O_2 + 0.714\ CH_3CHO + 0.714\ OH + H_2O$	$k_{34} = 1.13E\text{-}11\ \exp(55/T)$	4
K35)	$C_3H_8 + OH \rightarrow C_3H_7O_2 + H_2O$	$k_{35} = 1.50E\text{-}17\ T^2\ \exp(-44/T)$	4
K36)	$C_3H_7O_2 + NO \rightarrow NO_2 + 0.24\ C_2H_5O_2 + 0.09\ CH_3CHO + 0.18\ CO + 0.7\ CH_3COCH_3 + HO_2$	$k_{36} = 2.60E\text{-}17\ \exp(360/T)$	4
K37)	$C_3H_7O_2 + HO_2 \rightarrow C_3H_7OOH + O_2$	$k_{37} = 1.51E\text{-}13\ \exp(1300/T)$	4
K38)	$C_3H_7O_2 + CH_3O_2 \rightarrow 0.8\ C_2H_5O_2 + 0.3\ CH_3CHO + 0.6\ CO + 0.2\ CH_3COCH_3 + HO_2$	$k_{38} = 2.00E\text{-}13$	4
K39)	$C_3H_7OOH + OH \rightarrow 0.157\ C_3H_7O_2 + 0.142\ C_2H_5O_2 + 0.053\ CH_3CHO + 0.106\ CO + 0.666\ CH_3COCH_3 + 0.843\ OH + 0.157\ H_2O$	$k_{39} = 2.55E\text{-}11$	4
K40)	$CH_3COCH_3 + OH \rightarrow CH_3COCH_2O_2 + H_2O$	$k_{40} = 5.34E\text{-}18\ T^2\ \exp(-230/T)$	4
K41)	$CH_3COCH_2O_2 + NO \rightarrow NO_2 + CH_3COO_2 + CH_2O$	$k_{41} = 2.54E\text{-}12\ \exp(360/T)$	4
K42)	$CH_3COCH_2O_2 + NO_3 \rightarrow NO_2 + CH_3COO_2 + CH_2O$	$k_{42} = 2.50E\text{-}12$	4
K43)	$CH_3COCH_2O_2 + HO_2 \rightarrow HACET + O_2$	$k_{43} = 1.36E\text{-}13\ \exp(1250/T)$	4
K44)	$HACET + OH \rightarrow 0.323\ CH_3COCH_2O_2 + 0.677\ MGLY + 0.677\ OH$	$k_{44} = 9.20E\text{-}12$	4
	C_2H_4 and C_3H_6 Oxidation		
K45)	$C_2H_4 + OH + M \rightarrow HOC_2H_4O_2 + M$	$k_0 = 1.00E\text{-}28\ (300/T)^{0.8}$ $k_\infty = 8.80E\text{-}12$ $F_c = 0.6$	1
K46)	$C_2H_4 + O_3 \rightarrow CH_2O + 0.8\ CO + 0.2\ OH + 0.2\ HO_2 + 0.1\ H_2 + 0.2\ CO_2 + 0.4\ H_2O + 0.8\ O_2$	$k_{46} = 1.20E\text{-}14\ \exp(-2630/T)$	1
K47)	$HOC_2H_4O_2 + NO \rightarrow NO_2 + HO_2 + 2\ CH_2O$	$k_{47} = 9.00E\text{-}12$	2
K48)	$HOC_2H_4O_2 + HO_2 \rightarrow HOROOH + O_2$	$k_{48} = 6.50E\text{-}13\ \exp(650/T)$	5
K49)	$C_3H_6 + OH + M \rightarrow HOC_3H_6O_2 + M$	$k_0 = 8.00E\text{-}27\ (300/T)^{3.5}$ $k_\infty = 3.00E\text{-}11$ $F_c = 0.5$	2
K50)	$C_3H_6 + O_3 \rightarrow 0.5\ CH_2O + 0.5\ CH_3CHO + 0.36\ OH + 0.3\ HO_2 + 0.28\ CH_3O_2 + 0.56\ CO$	$k_{50} = 6.50E\text{-}15\ \exp(-1900/T)$	1
K51)	$HOC_3H_6O_2 + NO \rightarrow NO_2 + CH_3CHO + CH_2O + HO_2$	$k_{51} = 9.00E\text{-}12$	2
K52)	$HOC_3H_6O_2 + HO_2 \rightarrow HOROOH + O_2$	$k_{52} = 6.50E\text{-}13\ \exp(650/T)$	5
K53)	$HOROOH + OH \rightarrow 0.1\ HOC_2H_4O_2 + 0.05\ HOC_3H_6O_2 + 0.2\ CH_3COO_2 + 0.6\ CH_2O + 0.4\ CO + 0.85\ OH + H_2O$	$k_{53} = 3.80E\text{-}12\ \exp(200/T)$	5
	Other NMVOC Oxidation		
K54)	$ONMV + OH \rightarrow 0.5\ C_2H_5O_2 + 0.6\ ISO_2$	$k_{54} = 1.55E\text{-}11\ \exp(-540/T)$	5
	Acetaldehyde Degradation, etc.		
K55)	$CH_3CHO + OH \rightarrow CH_3COO_2 + H_2O$	$k_{55} = 5.60E\text{-}12\ \exp(270/T)$	1
K56)	$CH_3CHO + NO_3 \rightarrow CH_3COO_2 + HNO_3$	$k_{56} = 1.40E\text{-}12\ \exp(-1900/T)$	1
K57)	$CH_3COO_2 + NO \rightarrow NO_2 + CH_3O_2 + CO_2$	$k_{57} = 5.30E\text{-}12\ \exp(360/T)$	1
K58)	$CH_3COO_2 + NO_2 + M \rightarrow PAN + M$	$k_0 = 9.70E\text{-}29\ (300/T)^{5.6}$ $k_\infty = 9.30E\text{-}12\ (300/T)^{1.5}$ $F_c = 0.6$	1
K59)	$PAN + M \rightarrow CH_3COO_2 + NO_2 + M$	$k_{59} = k_{58}/(9.00E\text{-}29\ \exp(14000/T))$	1
K60)	$CH_3COO_2 + HO_2 \rightarrow CH_3COOOH + O_2$	$k_{60} = 4.50E\text{-}13\ \exp(1000/T)$ $/(1 + 1/(3.30E2\ \exp(-1430/T)))$	1
K61)	$CH_3COO_2 + HO_2 \rightarrow CH_3COOH + O_3$	$k_{61} = 4.50E\text{-}13\ \exp(1000/T)$ $/(1 + 3.30E2\ \exp(-1430/T))$	1
K62)	$CH_3COOOH + OH \rightarrow CH_3COO_2 + H_2O$	$k_{62} = 6.85E\text{-}12$	6
K63)	$CH_3COO_2 + CH_3O_2 \rightarrow CH_3O_2 + CH_2O + HO_2 + CO_2 + O_2$	$k_{63} = 1.30E\text{-}12\ \exp(640/T)$ $/(1 + 1/(2.20E6\ \exp(-3820/T)))$	1
K64)	$CH_3COO_2 + CH_3O_2 \rightarrow CH_3COOH + CH_2O + O_2$	$k_{64} = 1.30E\text{-}12\ \exp(640/T)$ $/(1 + 2.20E6\ \exp(-3820/T))$	1
K65)	$CH_3COO_2 + CH_3COO_2 \rightarrow 2\ CH_3O_2 + 2\ CO_2 + O_2$	$k_{65} = 2.90E\text{-}12\ \exp(500/T)$	1

Table 3. (continued)

No.	Reaction	Rate	Ref.
	C_5H_8 (Isoprene) and $C_{10}H_{16}$ (Terpene) Oxidation		
K66)	$C_5H_8 + OH \rightarrow ISO_2$	k_{66} = 2.45E-11 exp(410/T)	6
K67)	$C_5H_8 + O_3 \rightarrow 0.65$ MACR + 0.58 CH_2O + 0.1 $MACRO_2$ + 0.1 CH_3COO_2 + 0.08 CH_3O_2 + 0.28 HCOOH + 0.14 CO + 0.09 H_2O_2 + 0.25 HO_2 + 0.25 OH	k_{67} = 7.86E-15 exp(−1913/T)	6
K68)	$C_5H_8 + NO_3 \rightarrow$ ISON	k_{68} = 3.03E-12 exp(−446/T)	6
K69)	$ISO_2 + NO \rightarrow 0.956\ NO_2 + 0.956$ MACR + 0.956 CH_2O + 0.956 HO_2 + 0.044 ISON	k_{69} = 2.54E-12 exp(360/T)	6
K70)	$ISO_2 + HO_2 \rightarrow$ ISOOH	k_{70} = 2.05E-13 exp(1300/T)	6
K71)	$ISO_2 + ISO_2 \rightarrow 2$ MACR + CH_2O + HO_2	k_{71} = 2.00E-12	6
K72)	ISOOH + OH → MACR + OH	k_{72} = 1.00E-10	6
K73)	ISON + OH → ACETOL + NALD	k_{73} = 1.30E-11	6
K74)	MACR + OH → $MACRO_2$	k_{74} = 0.5 (4.13E-12 exp(452/T) + 1.86E-11 exp(175/T))	6
K75)	MACR + O_3 → 0.9 MGLY + 0.45 HCOOH + 0.32 HO_2 + 0.22 CO + 0.19 OH + 0.1 CH_3COO_2	k_{75} = 0.5 (1.36E-15 exp(−2112/T) + 7.51E-16 exp(−1521/T))	6
K76)	$MACRO_2$ + NO → NO_2 + 0.25 HACET + 0.25 CO + 0.25 CH_3COO_2 + 0.5 MGLY + 0.75 CH_2O + 0.75 HO_2	k_{76} = 2.54E-12 exp(360/T)	6
K77)	$MACRO_2 + HO_2 \rightarrow$ MACROOH	k_{77} = 1.82E-13 exp(1300/T)	6
K78)	$MACRO_2 + MACRO_2 \rightarrow$ HACET + MGLY + 0.5 CH_2O + 0.5 CO	k_{78} = 2.00E-12	6
K79)	$MACRO_2 + NO_2 + M \rightarrow$ MPAN + M	k_0 = 9.70E-29 (300/T)$^{5.6}$ k_∞ = 9.30E-12 (300/T)$^{1.5}$ F_c = 0.6	1
K80)	MPAN + M → $MACRO_2$ + NO_2 + M	$k_{80} = k_{79}$/(9.00E-29 exp(14000/T))	1
K81)	MPAN + OH → ACETOL + NO_2	k_{81} = 3.60E-12	4
K82)	MACROOH + OH → $MACRO_2$ + H_2O	k_{82} = 3.00E-11	6
K83)	MGLY + OH → CH_3COO_2 + CO	k_{83} = 1.50E-11	6
K84)	MGLY + NO_3 → CH_3COO_2 + CO + HNO_3	k_{84} = 1.44E-12 exp(−1862/T)	6
K85)	NALD + OH → CH_2O + CO + NO_2	k_{85} = 5.60E-12 exp(270/T)	6
K86)	$C_{10}H_{16}$ + OH → 1.5 ISO_2 + CH_3COCH_3	k_{86} = 1.20E-11 exp(444/T)	7
K87)	$C_{10}H_{16} + O_3 \rightarrow 1.3$ MACR + 1.16 CH_2O + 0.2 $MACRO_2$ + 0.2 CH_3COO_2 + 0.16 CH_3O_2 + 0.56 HCOOH + 0.28 CO + 0.18 H_2O_2 + 0.5 HO_2 + 0.5 OH	k_{87} = 9.90E-16 exp(−730/T)	5
K88)	$C_{10}H_{16} + NO_3 \rightarrow 1.2\ ISO_2 + NO_2$	k_{88} = 5.60E-11 exp(−650/T)	5

T, temperature (K); P_{atm}, pressure (atm); [M], air number density (cm^{-3}); [H_2O], water vapor density (cm^{-3}). The three-body reaction rates are computed by $k = (k_0[\mathrm{M}])/(1 + k_0[\mathrm{M}]/k_\infty)F_c^{1+\log_{10}\left(k_0[\mathrm{M}]/k_\infty\right)^2)^{-1}}$. References: 1, *Demore et al.* [1997]; 2, *Atkinson et al.* [2000]; 3, *Cantrell et al.* [1985]; 4, *Jenkin et al.* [1997]; 5, *Müller and Brasseur* [1995]; 6, *Pöschl et al.* [2000]; 7, *Carter* [1990].

South Africa, biomass burning emissions begin in May or June near the equator and shift southward with having a peak in October, whereas they begin in July in South America. Consequently, biomass burning emissions in South America are concentrated in August and September in comparison to South Africa. In South America, surface CO concentrations calculated by using this biomass burning emission seasonality have their peaks in September, in good agreement with observations in South America. CO has industrial emission sources as well as biomass burning emission. Figure 7 shows the distribution of CO surface emission. Large CO emission is found in industrial regions (principally America, Europe, China, and India) as emissions of other trace gases. Biomass burning emission is intensive in North Africa (January), in South America, and South Africa (September–October) as also seen in Figure 6. Additionally, there are indirect CO sources from the oxidation of methane and NMHCs (computed in the model). The global CO source from the methane and NMHCs oxidation is estimated at 1574 TgC/yr in CHASER (the detailed budget of the tropospheric CO in CHASER is shown by *Sudo et al.* [2002]).

[19] For NO_x, emissions from aircraft and lightning are considered as well as surface emission. Data for aircraft NO_x emission (0.55 TgN/yr) are taken from the EDGAR inventory. We assume that lightning NO_x production amounts to 5.0 TgN/yr in this study. In CHASER, lightning NO_x production is calculated in each time step using the parameterization of *Price and Rind* [1992] linked to the convection scheme of the AGCM. In the model, the proportions of could-to-ground (CG) flashes and intracloud (IC) flashes are calculated using the cloud top height determined from the AGCM convection scheme, following *Price et al.* [1997] (NO_x production by CG flashes is assumed to be 10 times as efficient as by IC flashes). Computed lightning NO_x emission is redistributed vertically by updrafts and downdrafts in the AGCM convection scheme after distributed uniformally in the vertical. As a consequence, computed lightning NO_x emission is transported to the upper tropospheric layers and fractionally to the lower layers in the model (leading to C-shape profiles) as studied by *Pickering et al.* [1998]. The distributions of aircraft and lightning NO_x emission in the model are shown in Figure 8. The aircraft emission seems to have an importance for the NO_x budget in the northern mid high latitudes especially in wintertime. The lightning emission is generally intensive over the continent in the summer-hemisphere. In July, lightning NO_x production is most intensive in the monsoon region like southeastern Asia and North Africa where convective activity is high in this season. NO_x also has a emission source from soils (5.5 TgN/yr). Soil NO_x emission is prescribed using monthly data for soil NO_x emission from *Yienger and*

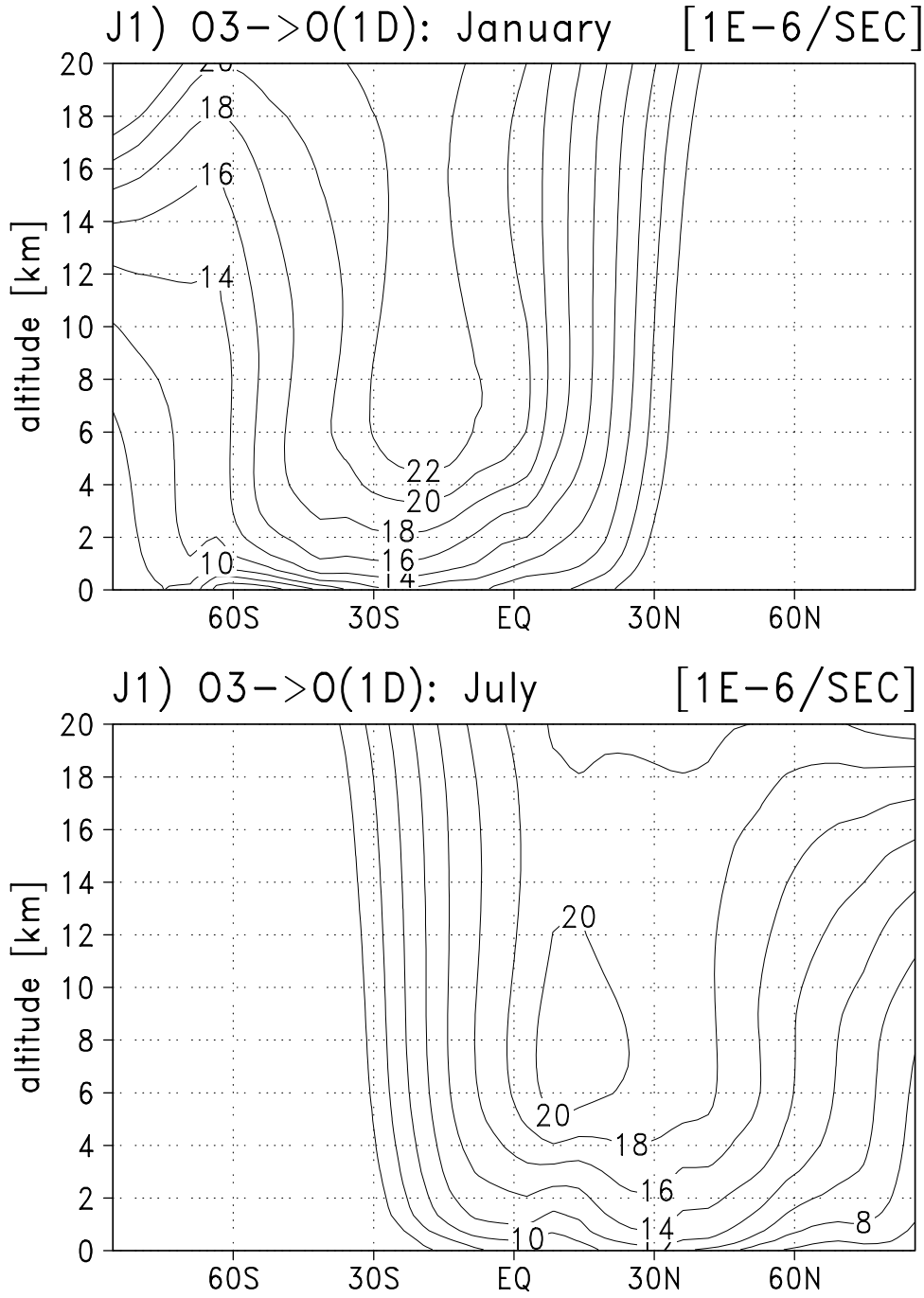

Figure 5. Zonally averaged photolysis rate (sec^{-1}) of O_3 to $O(^1D)$ photolysis calculated for January and July.

Table 4. Global Emissions of Trace Gases Considered in CHASER

	NO_x	CO	C_2H_6	C_3H_8	C_2H_4	C_3H_6	CH_3COCH_3	ONMV	C_5H_8	$C_{10}H_{16}$
Industry	23.10	337.40	3.15	5.76	2.00	0.85	1.02	29.20	0.00	0.00
B.B.[a]	9.65	889.40	4.50	2.62	14.10	6.39	7.17	8.55	0.00	0.00
Vegetation	0.00	0.00	1.20	1.60	4.30	1.20	11.20	20.00	400.00	102.00
Ocean	0.00	0.00	0.10	0.11	8.28	10.10	0.00	2.00	0.00	0.00
Soil	5.50	0.00	0.00	0.00	0.00	0.00	0.00	0.00	0.00	0.00
Lightning	5.00	0.00	0.00	0.00	0.00	0.00	0.00	0.00	0.00	0.00
Aircraft	0.55	0.00	0.00	0.00	0.00	0.00	0.00	0.00	0.00	0.00
Total	43.80	1226.80	8.95	10.09	28.68	18.54	19.39	59.75	400.00	102.00

Units are TgN/yr for NO_x, TgCO/yr for CO, and TgC/yr for NMHCs.
[a]Biomass burning.

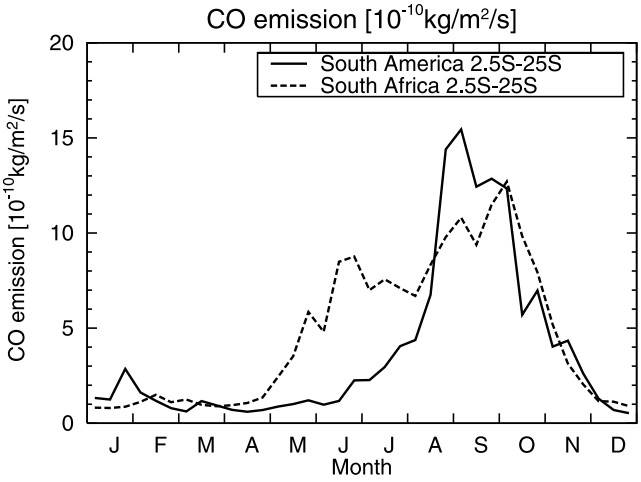

Figure 6. Seasonal variations of CO surface emission averaged over South America (2.5°S–25°S) and South Africa (2.5°S–25°S) in the model.

Levy [1995], obtained via the Global Emissions Inventory Activity (GEIA) [*Graedel et al.*, 1993].

[20] Biogenic emissions from vegetation are considered for NMHCs. The monthly data by *Guenther et al.* [1995], obtained via the GEIA inventory, are used for isoprene, terpenes, ONMV, and other NMHCs emissions. Isoprene emission and terpenes emission are reduced by 20% to 400 TgC/yr and 102 TgC/yr, respectively following *Houweling et al.* [1998] and *Roelofs and Lelieveld* [2000]. The diurnal cycle of isoprene emission is simulated using solar incidence at the surface. For terpenes emission, the diurnal cycle is parameterized using surface air temperature in the model [*Guenther et al.*, 1995]. Figure 9 shows the distributions of isoprene emission for January and July in the model. In July, isoprene emission is large through much of the continent in the northern hemisphere, with showing significant values in the eastern United States and eastern Asia.

6. Depositions

[21] Deposition processes significantly affect the distribution and budget of trace gas species (e.g., O_3, NO_x, HO_x). The CHASER model considers dry deposition at the surface and wet scavenging by precipitation.

6.1. Dry Deposition

[22] In CHASER, dry deposition scheme is largely based on a resistance series parameterization of *Wesely* [1989] and applied for ozone (O_x), NO_x, HNO_3, HNO_4, PAN, MPAN, ISON, H_2O_2, CO, CH_3COCH_3, CH_2O, MGLY, MACR, HACET, and peroxides like CH_3OOH (see Table 1) in this study. Dry deposition velocities (v_d) for the lowermost level of the model are computed as

$$v_d = \frac{1}{r_a + r_b + r_s} \tag{1}$$

where r_a, r_b, r_s are the aerodynamic resistance, the surface canopy (quasi-laminar) layer resistance, and the surface resistance, respectively. r_a has no species dependency and is calculated using surface wind speed and bulk coefficient computed for the model's lowest level in the AGCM. r_b is calculated using friction velocity computed in the AGCM and the Shumid number (calculated with the kinematic viscosity of air and the diffusive coefficient for individual species). Finally, the most important resistance r_s is calculated as a function of surface (vegetation) type over land and species using temperature, solar influx, precipitation, snow cover ratio, and the effective Henry's law constant calculated for individual species in the AGCM. r_s over sea and ice surface are taken to be the values used by *Brasseur et al.* [1998] (e.g., $v_d(O_3) = 0.075$ cm s^{-1} over sea and ice). The effect of dry deposition on the concentration of each trace gas in the lowest layer is evaluated together with surface emissions and vertical diffusion by solving the diffusion equations implicitly.

[23] Figure 10 shows the calculated 24-hour average deposition velocities (cm s^{-1}) of ozone in January and July. The values show the deposition velocities calculated for the surface elevation. Deposition velocities of ozone are generally higher than 0.1 cm s^{-1}, except for the high latitudes in winter where solar influx is less intense and much of the surface is covered with snow. In July, ozone deposition velocity ranges from 0.2 to 0.5 cm s^{-1} over land surface in the northern hemisphere (0.3–0.7 cm s^{-1} in daytime), in good agreement with the observations [*Jacob et al.*, 1992; *Van Pul*, 1992; *Massman et al.*, 1994; *Ritter et al.*, 1994]. In the tropical rain forest region (e.g., the Amazon Forest), deposition velocities are high with a range of 0.7–1.2 cm s^{-1} throughout a year, in agreement with the observations [*Fan et al.*, 1990].

6.2. Wet Deposition

[24] Wet deposition is considered in two different ways in the model; in-cloud scavenging (rain-out) and below-cloud scavenging (wash-out). A choice of species which are subject to wet deposition is determined from their effective Henry's law constant in standard conditions (H_s, $T = 298.15$ K). In the present model configuration, in-cloud scavenging is applied for species whose H_s are greater than 10^2 M atm^{-1}, and additionally below-cloud scavenging is also applied if H_s is greater than 10^4 M atm^{-1}. In this study, in-cloud scavenging is applied for H_2O_2, HNO_3, HNO_4, CH_2O, MGLY, HACET, ISON, and peroxides (CH_3OOH, C_2H_5OOH, etc.), with below-cloud scavenging for H_2O_2, HNO_3, and HNO_4.

[25] For in-cloud scavenging, the first-order parameterization of *Giorgi and Chameides* [1985] is employed. The loss rate β (s^{-1}) due to in-cloud scavenging is calculated by

$$\beta = \frac{P}{Q_L + D_{\mathrm{H_2O}}/(H\ RT)} \tag{2}$$

where P is the precipitation production rate (g cm^{-3} s^{-1}) due to convective precipitation and large-scale condensation, Q_L is the liquid water content (g cm^{-3}), $D_{\mathrm{H_2O}}$ is the density of liquid water (=1 g cm^{-3}), R is the gas constant (=0.082 atm M^{-1} K^{-1}), and H is the effective Henry's law constant (M atm^{-1}) of each species calculated as a function of temperature T (K). P, Q_L, and T are calculated by the AGCM.

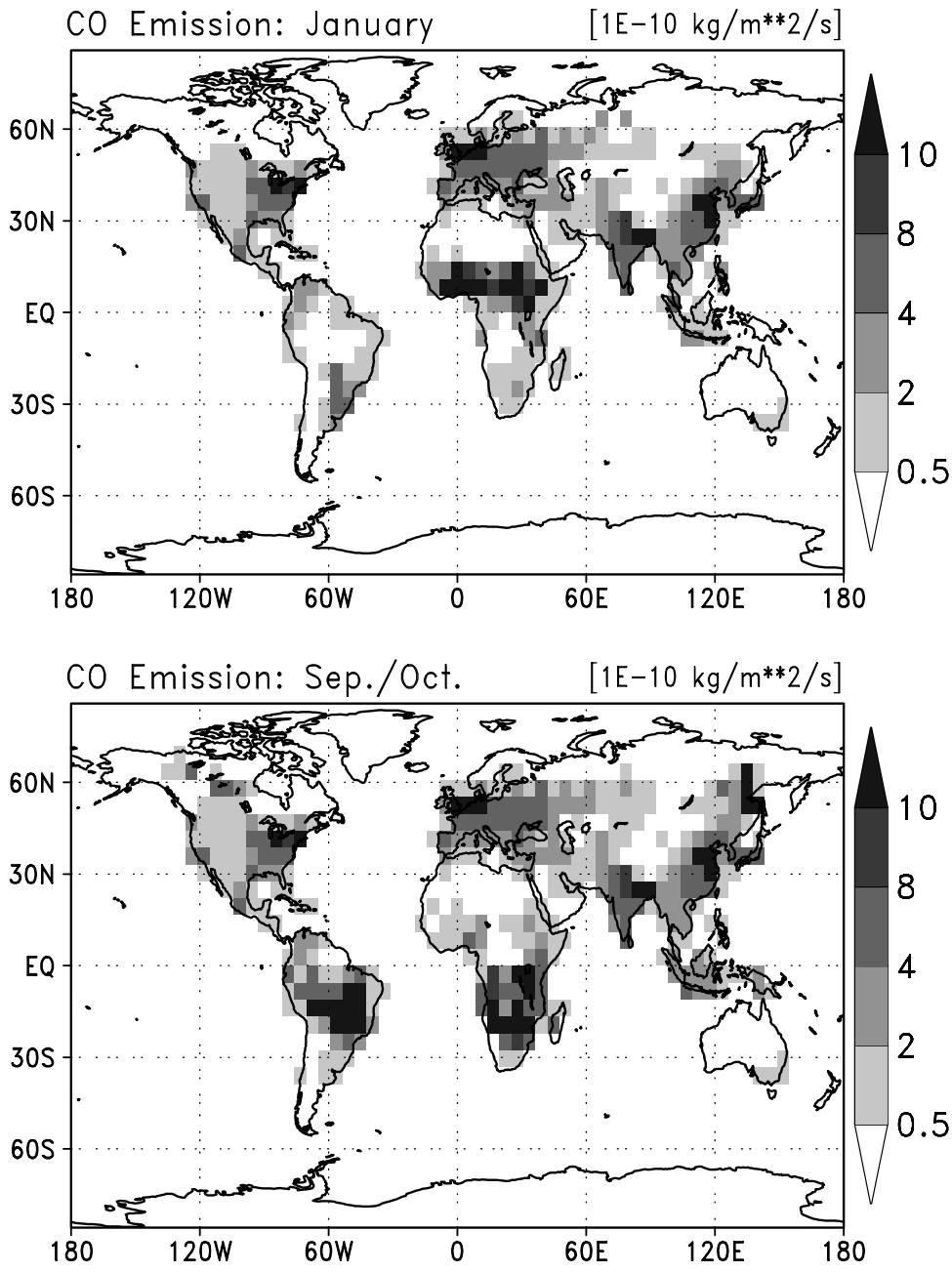

Figure 7. Distribution of CO surface emission in January average and September–October average.

[26] In the case of below-cloud scavenging for HNO_3, HNO_4 and H_2O_2, irreversible scavenging is assumed, and the loss rate associated with below-cloud scavenging is given by

$$\beta = \frac{6K_g(d)Q_R}{D_{H_2O}d} \tag{3}$$

where d is the effective raindrop diameter (cm) calculated according to *Mason* [1971] and *Roelofs and Lelieveld* [1995], Q_R is the raindrop density (g cm^{-3}) determined from the precipitation flux (intensity) calculated for individual model levels in the AGCM, K_g is the mass transfer coefficient of a gaseous molecule to a sphere and calculated by an empirical correlation [e.g., *Frössling*, 1938] as a function of the raindrop diameter d, the kinematic viscosity of air, the diffusive coefficients, and the terminal velocity of raindrops (computed using an empirical relation to the raindrop diameter d). The below-cloud scavenging scheme is applied with respect to convective precipitation and large-scale precipitation separately.

[27] The calculated loss rates (day^{-1}) of HNO_3 due to wet deposition (in-cloud and below-could scavenging) are shown in Figure 11 (zonal mean) as an example. Wet deposition is efficient in the tropics and the midlatitudes for both seasons, associated with the convective activity and the passage of cyclones (migratory cyclones-anticyclones). In January, high scavenging rates leading to a lifetime of 0.5–1.5 days are simulated over South America, South Africa, and the western Pacific including Indonesia and

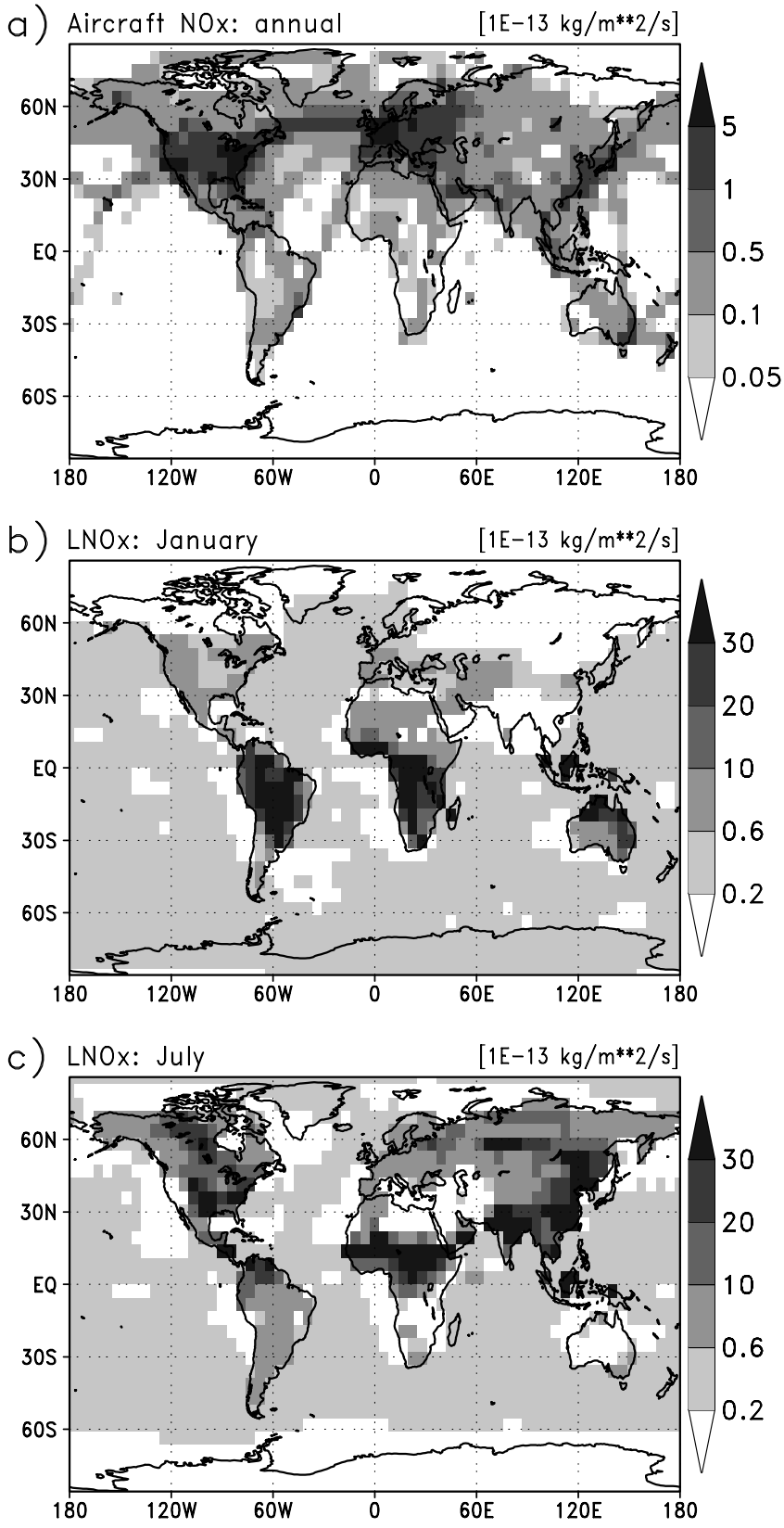

Figure 8. Distribution of aircraft and lightning NO_x emission (column total) in CHASER. (a) Aircraft emission (annual mean). (b), (c) Lightning emission calculated for January and July, respectively.

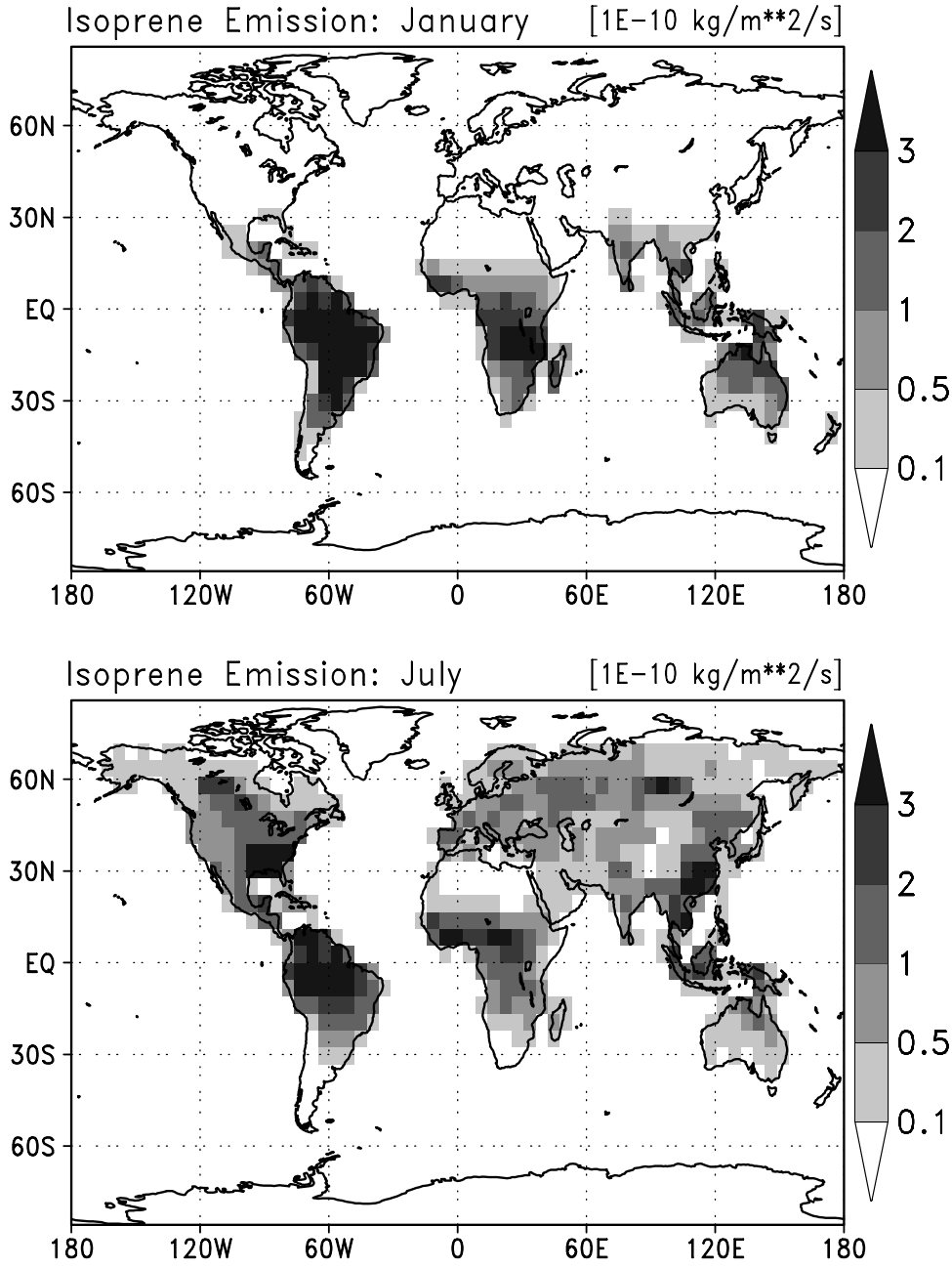

Figure 9. Distribution of isoprene (C_5H_8) surface emission for January and July.

the north part of Australia in the low latitudes of 0°–20°S (not shown), whereas wet deposition is much less intensive in the air descending region as over the southern Atlantic and the southeastern Pacific because of sparse precipitation. In July, wet deposition is most intensive over southeastern Asia from India to China associated with the monsoon circulation, leading to a lifetime of 0.3–1 days in the middle troposphere.

[28] For an evaluation of the wet deposition scheme described here, we have conducted a simulation using atmospheric lead (^{210}Pb) as a tracer. This simulation has been performed as an extension of the simulation of ^{222}Rn (section 3), because ^{210}Pb is produced by radioactive decay of ^{222}Rn. ^{210}Pb produced from ^{222}Rn, believed to stick to aerosol surfaces rapidly, was assumed to efficiently removed by wet deposition with the same scavenging lifetime for HNO_3 as in many other simulations [*Balkanski et al.*, 1993; *Lee and Feichter*, 1995; *Rehfeld and heimann*, 1995; *Brasseur et al.*, 1998]. The dry deposition velocity of ^{210}Pb at the surface is taken to be 0.2 cm s^{-1} over land surface and 0.05 cm s^{-1} over sea surface, following *Balkanski et al.* [1993].

[29] Figure 12 shows a comparison of the mixing ratios of ^{210}Pb calculated and observed at the surface. The seasonal variations of ^{210}Pb are well reproduced by the model for all sites. For Mauna Loa, calculated values are in good agreement with the observation because of our augmentation of radon emission in eastern Asia (see section 3). Although Figure 12 indicates that the model successfully simulates the wet deposition process, it

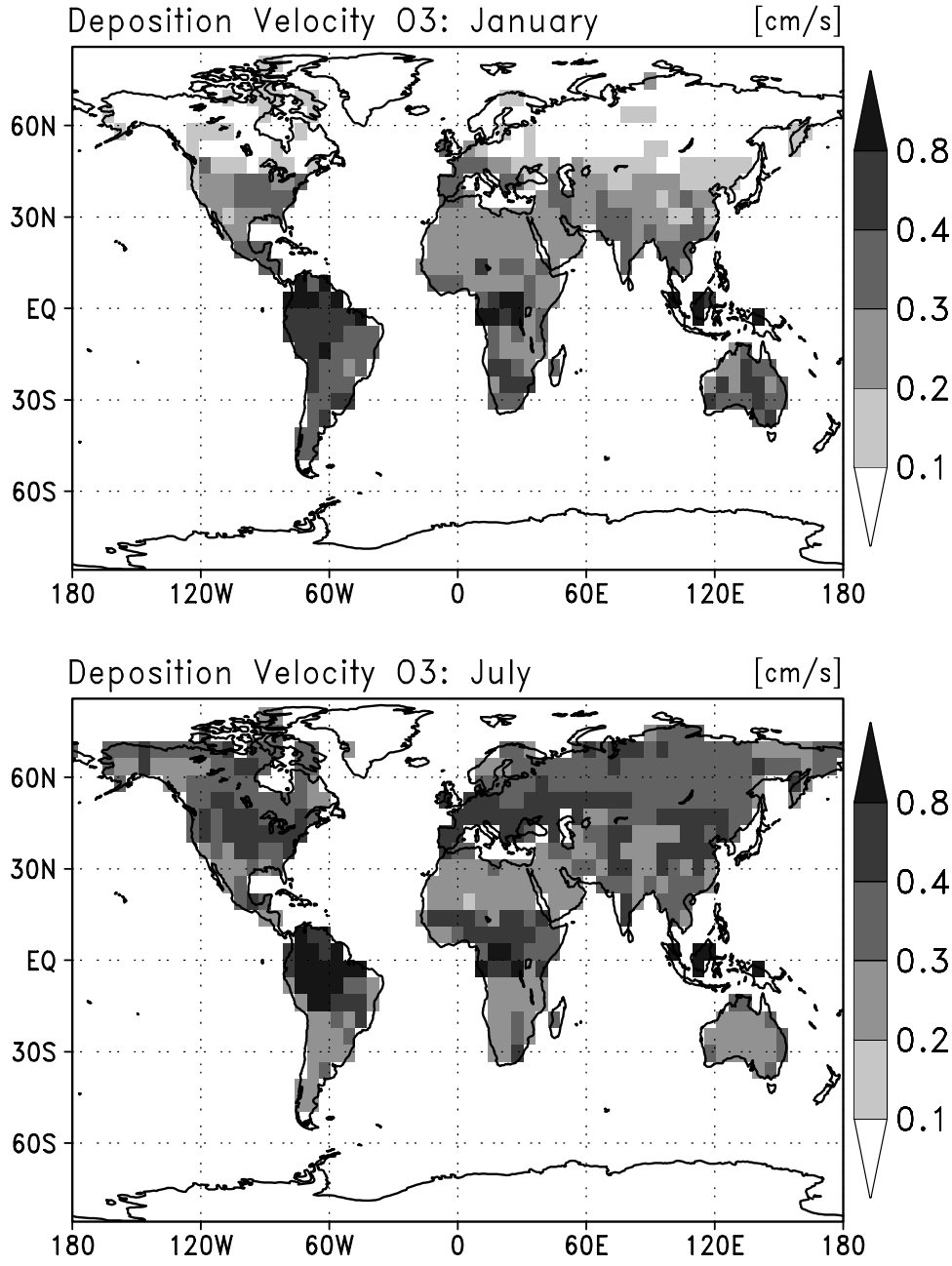

Figure 10. Calculated 24-hour average deposition velocities (cm/s) for ozone at the surface in January and July.

should be noted that there may be uncertainties in the surface emission of radon adopted here and precipitation simulated by the AGCM.

[30] Wet deposition is one of the most important processes, and is the most difficult process to simulate. Therefore, a further development of the wet deposition scheme is needed. *Velders and Granier* [2001] show that tropospheric chemistry in atmospheric chemistry transport models has some sensitivities to the wet deposition parameterization used in them. The two kinds of parameterizations for in-cloud and below-cloud scavenging used in this study are basically identical to those adopted in the MOZART model [*Brasseur et al.*, 1998]. We are developing more detailed schemes for wet deposition; for example, below-cloud scavenging linked to the cumulus convection scheme of the AGCM, reemission process of solved species due to reevaporation of raindrops, and deposition on ice particles like cirrus [*Lawrence and Crutzen*, 1998; *Lawrence et al.*, 1999], though sedimentation (gravitational settling) of ice particles is included in the precipitation production rate P in (2).

7. Conclusions

[31] We have presented a new global three-dimensional chemical model for the troposphere, named CHASER.

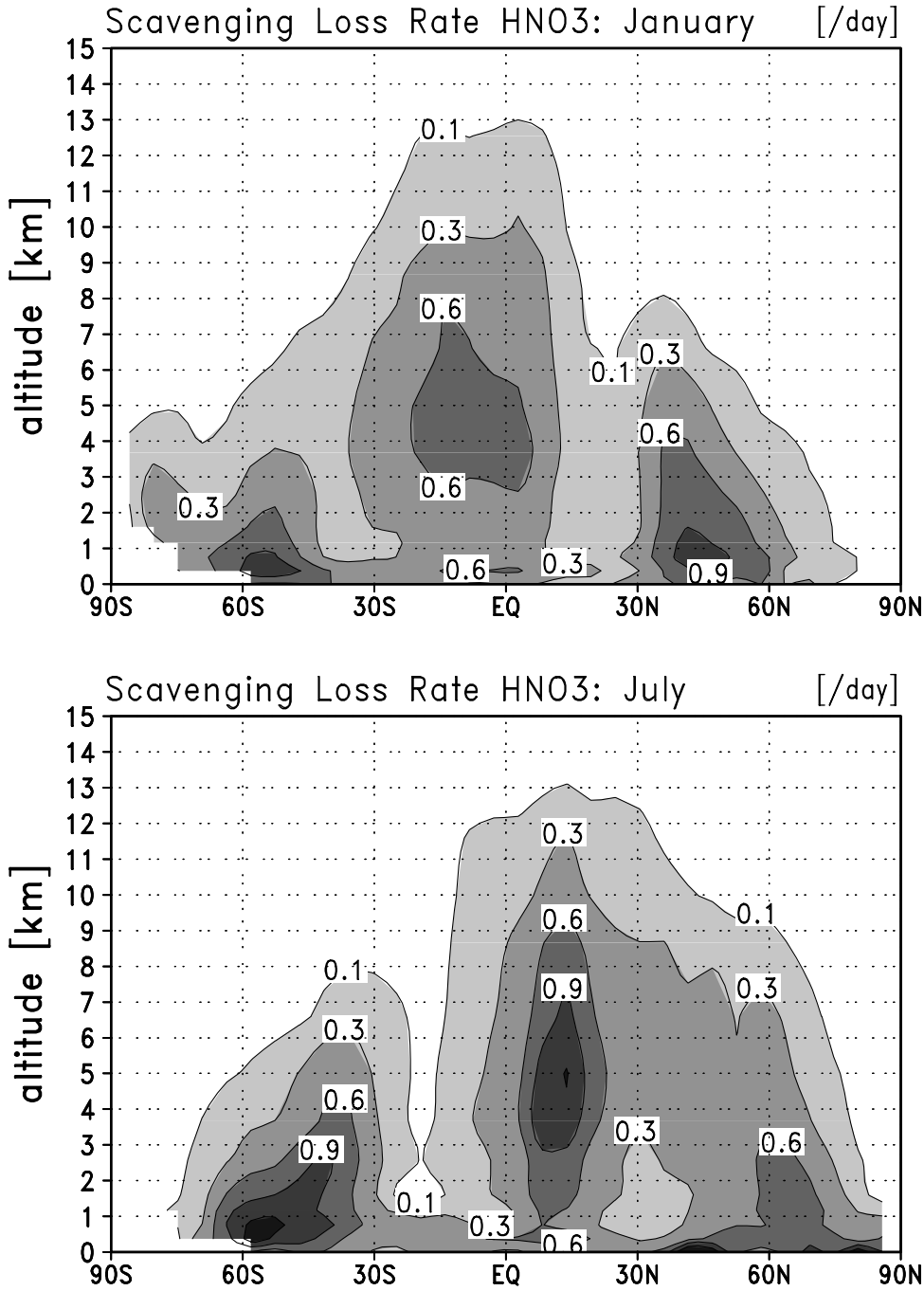

Figure 11. Simulated loss rate (day^{-1}) of HNO_3 due to wet deposition for January and July.

The model has been developed, aimed at studying the global distributions and budgets of tropospheric ozone and related gases, and the radiative effect of tropospheric ozone on climate. The model simulates the major processes involving tropospheric photochemistry such as large-scale and subgrid-scale transport, emissions, deposition, and chemical transformations. Transport, deposition, and other dynamical or physical processes are simulated on-line by the CCSR/NIES AGCM with a typical time step of 30 min. The concentration of chemical species (mainly ozone) calculated by the chemistry component of the model is used for the radiation calculation of the AGCM. In this study, we adopted a horizontal resolution of T21 (5.6° × 5.6°) with a relatively high vertical resolution (32 layers from the surface up to about 3 hPa), though the model can run with a higher horizontal resolution like T42 (2.8° × 2.8°) or higher. Though the T21 horizontal resolution adopted in this study is computationally efficient and may be fairly adequate to simulate global tropospheric photochemistry, we are going to conduct simulations with a higher horizontal resolution for an accurate representation of individual processes (especially

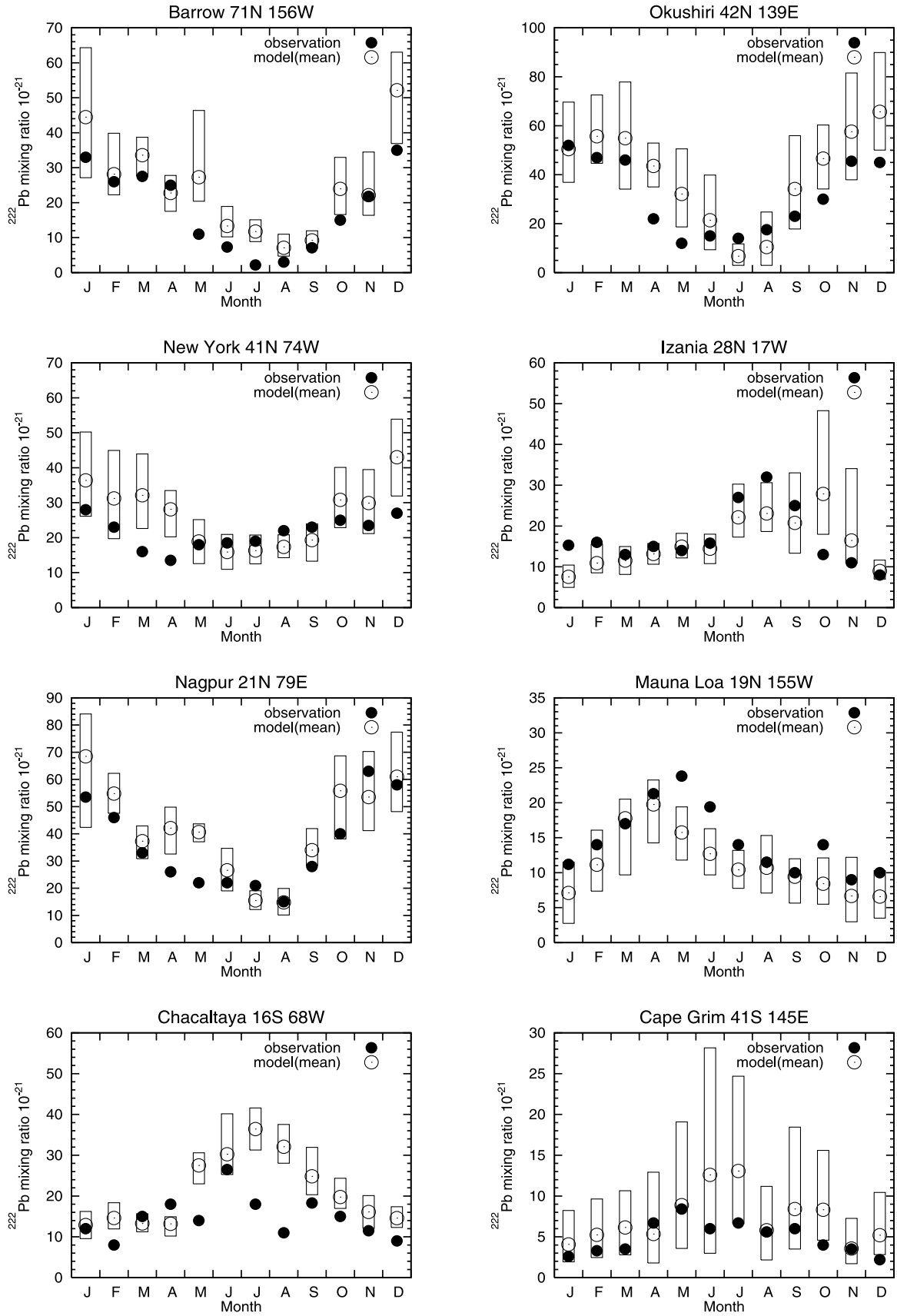

Figure 12. Seasonal variations of calculated (open circles) and observed (filled circles) surface lead (^{210}Pb). Boxes show the range of calculated values.

of transport) and for detailed analysis and evaluation of the model results.

[32] In this paper, the transport scheme and the deposition scheme used in the model are evaluated by conducting a simple simulation of ^{222}Rn and ^{210}Pb. The results suggest that the model is capable of simulating long-range transport such as Asian outflow reaching to the United States. Though the evaluation of the deposition scheme shows that the model simulates deposition processes well, more detailed scheme for dry and wet deposition will be implemented in the next version of the model.

[33] The chemistry component of the model accounts for 88 kinetic reactions and 25 photolytic reactions with 47 chemical species in the present configuration. Heterogeneous reactions on aerosols related to NO_x, HO_x, and some peroxy radicals (RO_2), not considered in the present model version, will be included in the next model version.

[34] The model results are evaluated and discussed by a companion paper [*Sudo et al.*, 2002].

[35] **Acknowledgments.** We are grateful to M. Takigawa for providing output data from his three-dimensional stratospheric chemical model. We wish to thank K. Toyota and M. Capouet for invaluable comments and discussions. We would like to give special thanks to the late Atusi Numaguti (main developer of the CCSR/NIES AGCM) for many discussions. We dedicate this study to the memory of Atusi Numaguti. This work has been supported by Center for Climate System Research of the University of Tokyo and Frontier Research System for Global Change. Comments on the manuscript by two anonymous reviewers are greatly appreciated.

References

Arino, O., J.-M. Rosaz, and J.-M. Melinotte, World Fire Atlas with AVHRR and ATSR, paper presented at IUFRO Conference on Remote Sensing and Forest Monitoring, Rogow, Poland, 1999.

Atkinson, R., D. L. Baulch, R. A. Cox, R. F. Hampson, J. A. Kerr, M. J. Rossi, and J. Troe, Evaluated kinetic and photochemical data for atmospheric chemistry: Supplement VII — IUPAC subcommittee on gas kinetic data evaluation for atmospheric chemistry, *J. Phys. Chem. Ref. Data*, *28*, 191–393, 1999.

Atkinson, R., D. L. Baulch, R. A. Cox, R. F. Hampson, J. A. Kerr, and M. J. Rossi, Evaluated kinetic and photochemical data for atmospheric chemistry: Supplement VIII — IUPAC subcommittee on gas kinetic data evaluation for atmospheric chemistry, *J. Phys. Chem. Ref. Data*, *29*, 167–266, 2000.

Balkanski, Y. Y., D. J. Jacob, and G. M. Gardner, Transport and residence times of tropospheric aerosols inferred from a global three-dimensional simulation of ^{210}Pb, *J. Geophys. Res.*, *98*, 20,573–20,586, 1993.

Berntsen, T. K., and I. S. A. Isaksen, A global three-dimensional chemical transport model for the troposphere, *J. Geophys. Res.*, *102*, 21,239–21,280, 1997.

Brasseur, G. P., D. A. Hauglustaine, S. Walters, and P. J. Rasch, MOZART, a global chemical transport model for ozone and related chemical tracers, 1, Model description, *J. Geophys. Res.*, *103*, 28,265–28,289, 1998.

Cantrell, C. A., W. R. Stockwell, L. G. Anderson, K. L. Busarow, D. Perner, A. Schmeltekopf, J. G. Calvert, and H. S. Johnston, Kinetic study of the NO_3-CH_2O reaction and its possible role in nighttime tropospheric chemistry, *J. Phys. Chem.*, *89*, 139–146, 1985.

Carter, W., A detailed mechanism for the gas-phase atmospheric reactions of organic compounds, *Atmos. Environ., Part A*, *24*, 481–518, 1990.

Crutzen, P. J., and P. H. Zimmermann, The changing photochemistry of the troposphere, *Tellus*, *43*, 136–151, 1991.

DeMore, W. B., S. P. Sander, D. M. Golden, R. F. Hampson, M. J. Kurylo, C. J. Howard, A. R. Ravishankara, C. E. Kolb, and M. J. Molina, *Chemical Kinetics and Photochemical Data for Use in Stratospheric Modeling, JPL Publ. 97-4*, Jet Propul. Lab., Pasadena, Calif., 1997.

Dentener, F. J., and P. Crutzen, Reaction of N_2O_5 on tropospheric aerosols: impact on the global distributions of NO_x, O_3, and OH, *J. Geophys. Res.*, *98*, 7149–7162, 1993.

Fan, S. M., S. C. Wofsy, P. S. Bakwin, D. J. Jacob, and D. R. Fzjarrald, Atmosphere-biosphere exchange of CO_2 and O_3 in the Central Amazon Forest, *J. Geophys. Res.*, *95*, 16,851–16,864, 1990.

Frössling, N., The evaporating of falling drops, *Beitr. Geophys.*, *52*, 170–216, 1938.

Gierczak, T., J. B. Burkholder, S. Bauerle, and A. R. Ravishankara, Photochemistry of acetone under tropospheric conditions, *Chem. Phys.*, *231*, 229–244, 1998.

Giorgi, F., and W. L. Chameides, The rainout parameterization in a photochemical model, *J. Geophys. Res.*, *90*, 7872–7880, 1985.

Graedel, T. E., et al., A compilation of inventories of emissions to the atmosphere, *Global Biogeochem. Cycles*, *7*, 1–26, 1993.

Guenther, A., et al., A global model of natural volatile organic compound emissions, *J. Geophys. Res.*, *100*, 8873–8892, 1995.

Hao, W. M., and M.-H. Liu, Spatial distribution of tropical biomass burning in 1980 with $5^\circ \times 5^\circ$ resolution, *Global Biogeochem. Cycles*, *8*, 495–503, 1994.

Hauglustaine, D. A., G. P. Brasseur, S. Walters, P. J. Rasch, J.-F. Müller, L. K. Emmons, and M. A. Carroll, MOZART, a global chemical transport model for ozone and related chemical tracers, 2, Model results and evaluation, *J. Geophys. Res.*, *103*, 28,291–28,335, 1998.

Haywood, J. M., M. D. Schwarzkopf, and V. Ramaswamy, Estimates of radiative forcing due to modeled increases in tropospheric ozone, *J. Geophys. Res.*, *103*, 16,999–17,007, 1998.

Hertel, O., R. Berkowicz, and J. Christensen, Test of two numerical schemes for use in atmospheric transport-chemistry models, *Atmos. Environ., Part A*, *27*, 2591–2611, 1993.

Houweling, S., F. Dentener, and J. Lelieveld, Impact of nonmethane hydrocarbon compounds on tropospheric photochemistry, *J. Geophys. Res.*, *103*, 10,673–10,696, 1998.

Jacob, D. J., Heterogeneous chemistry and tropospheric ozone, *Atmos. Environ.*, *34*, 2131–2159, 2000.

Jacob, D. J., et al., Deposition of ozone to tundra, *J. Geophys. Res.*, *97*, 16,473–16,479, 1992.

Jacob, D. J., et al., Evaluation and intercomparison of global atmospheric transport models using ^{222}Rn and other short-lived tracers, *J. Geophys. Res.*, *102*, 5953–5970, 1997.

Jaeglé, L., et al., Photochemistry of HO_x in the upper troposphere at northern midlatitudes, *J. Geophys. Res.*, *105*, 3877–3892, 1999.

Jenkin, M. E., S. M. Saunders, and M. J. Pilling, The tropospheric degradation of volatile organic compounds: A protocol for mechanism development, *Atmos. Environ.*, *31*, 81–104, 1997.

Kritz, M. A., S. W. Rosner, and D. Z. Stockwell, Validation of an off-line three-dimensional chemical transport model using observed radon profiles, 1, Observations, *J. Geophys. Res.*, *103*, 8425–8432, 1998.

Landgraf, J., and P. J. Crutzen, An efficient method for online calculations of photolysis and heating rates, *J. Atmos. Sci.*, *55*, 863–878, 1998.

Lawrence, M. G., and P. J. Crutzen, The impact of cloud particle gravitational settling on soluble trace gas distributions, *Tellus, Ser. B*, *50*, 263–289, 1998.

Lawrence, M. G., P. J. Crutzen, P. J. Rasch, B. E. Eaton, and N. M. Mahowald, A model for studies of tropospheric photochemistry: Description, global distributions, and evaluation, *J. Geophys. Res.*, *104*, 26,245–26,277, 1999.

Lee, H. N., and J. Feichter, An intercomparison of wet precipitation scavenging schemes and the emission rates of ^{222}Rn for the simulation of global transport and deposition of ^{210}Pb, *J. Geophys. Res.*, *100*, 23,253–23,270, 1995.

Levy, H., II, J. D. Mahlman, and W. J. Moxim, Tropospheric ozone: The role of transport, *J. Geophys. Res.*, *90*, 3753–3772, 1985.

Lin, S.-J., and R. B. Rood, Multidimensional flux-form semi-Lagrangian transport schemes, *Mon. Weather Rev.*, *124*, 2046–2070, 1996.

Mahowald, N. M., P. J. Rasch, B. E. Eaton, S. Wittlestone, and R. G. Prinn, Transport of ^{222}Radon to the remote troposphere using MATCH and assimilated winds from ECMWF and NCEP/NCAR, *J. Geophys. Res.*, *102*, 28,139–28,152, 1997.

Mason, B. J., *The Physics of Clouds*, Clarendon, Oxford, England, 1971.

Massman, W. J., J. Pederson, A. Delany, D. Grantz, G. den Hartog, H. H. Neumann, S. P. Oncley, and R. Pearson Jr., An evaluation of the regional acid deposition model surface module for ozone uptake at three sites in the San Joaquin Valley of California, *J. Geophys. Res.*, *99*, 8281–8294, 1994.

McFarlane, N. A., The effect of orographically excited gravity wave drag on the general circulation of the lower stratosphere and troposphere, *J. Atmos. Sci.*, *44*, 1775–1800, 1987.

Mellor, G. L., and T. Yamada, A hierarchy of turbulence closure models for planetary boundary layers, *J. Atmos. Sci.*, *31*, 1791–1806, 1974.

Mickley, L. J., D. J. Jacob, and D. Rind, Uncertainty in preindustrial abundance of tropospheric ozone: Implications for radiative forcing calculations, *J. Geophys. Res.*, *106*, 3389–3399, 2001.

Müller, J.-F., Geographical distribution and seasonal variation of surface

emissions and deposition velocities of atmospheric trace gases, *J. Geophys. Res.*, *97*, 3787–3804, 1992.

Müller, J.-F., and G. P. Brasseur, IMAGES: A three-dimensional chemical transport model of the global troposphere, *J. Geophys. Res.*, *100*, 16,445–16,490, 1995.

Nakajima, T., and M. Tanaka, Matrix formulation for the transfer of solar radiation in a plane-parallel scattering atmosphere, *J. Quant. Spectrosc. Radiat. Transfer*, *35*, 13–21, 1986.

Nakajima, T., M. Tsukamoto, Y. Tsusima, and A. Numaguti, Modeling of the radiative process in a AGCM, in *Reports of a New Program for Creative Basic Research Studies, Studies of Global Environment Change With Special Reference to Asia and Pacific Regions, Rep. I-3*, pp. 104–123, CCSR, Tokyo, 1995.

Numaguti, A., Dynamics and energy balance of the hadley circulation and the tropical precipitation zones: Significance of the distribution of evaporation, *J. Atmos. Sci.*, *50*, 1874–1887, 1993.

Numaguti, A., Origin and recycling processes of precipitating water over the Eurasian continent: Experiments using an atmospheric general circulation model, *J. Geophys. Res.*, *104*, 1957–1972, 1999.

Numaguti, A., M. Takahashi, T. Nakajima, and A. Sumi, Development of an atmospheric general circulation model, in *Reports of a New Program for Creative Basic Research Studies, Studies of Global Environment Change With Special Reference to Asia and Pacific Regions, Rep. I-3*, pp. 1–27, CCSR, Tokyo, 1995.

Olivier, J. G. J., et al., Description of EDGAR Version 2.0. A set of global emission inventories of greenhouse gases and ozone-depleting substances for all anthropogenic and most natural sources on a per country basis and on 1o × 1o grid, *RIVM Rep. 771060 002/TNO*, Natl. Inst. for Public Health and the Environ., Bilthoven, Netherlands, 1996.

Pickering, K. E., Y. Wang, W.-K. Tao, C. Price, and J.-F. Müller, Vertical distributions of lightning NO_x for use in regional and global chemical transport models, *J. Geophys. Res.*, *103*, 31,203–31,216, 1998.

Pöschl, U., R. von Kuhlmann, N. Poisson, and P. J. Crutzen, Development and intercomparison of condensed isoprene oxidation mechanisms for global atmospheric modeling, *J. Atmos. Chem.*, *37*, 29–52, 2000.

Price, C., and D. Rind, A simple lightning parameterization for calculating global lightning distributions, *J. Geophys. Res.*, *97*, 9919–9933, 1992.

Price, C., J. Penner, and M. Prather, NO_x from lightning, 1, Global distribution based on lightning physics, *J. Geophys. Res.*, *102*, 5929–5941, 1997.

Randel, W. J., Seasonal cycles and QBO variations in stratospheric CH_4 and H_2O observed in UARS HALOE data, *J. Atmos. Sci.*, *55*, 163–185, 1998.

Rehfeld, S., and M. Heimann, Three dimensional atmospheric transport simulation of the radioactive tracers ^{210}Pb, ^{7}Be, ^{10}Be, and ^{90}Sr, *J. Geophys. Res.*, *100*, 26,141–26,161, 1995.

Ritter, J. A., J. D. Barrick, C. E. Watson, G. W. Sachse, G. L. Gregory, B. E. Anderson, M. A. Woerner, and J. E. Collins Jr., Airborne boundary layer flux measurements of trace gas species over Canadian boreal forest and northern wetland regions, *J. Geophys. Res.*, *99*, 1671–1685, 1994.

Roelofs, G.-J., and J. Lelieveld, Distribution and budget of O_3 in the troposphere calculated with a chemistry general circulation model, *J. Geophys. Res.*, *100*, 20,983–20,998, 1995.

Roelofs, G.-J., and J. Lelieveld, Tropospheric ozone simulation with a chemistry-general circulation model: Influence of higher hydrocarbon chemistry, *J. Geophys. Res.*, *105*, 22,697–22,712, 2000.

Roelofs, G.-J., J. Lelieveld, and R. van Dorland, A three-dimensional chemistry/general circulation model simulation of anthropogenically derived ozone in the troposphere and its radiative climate forcing, *J. Geophys. Res.*, *102*, 23,389–23,401, 1997.

Russel, J. M., III, et al., The halogen occultation experiment, *J. Geophys. Res.*, *98*, 10,777–10,798, 1993.

Sander, S. P., et al., *Chemical Kinetics and Photochemical Data for Use in Stratospheric Modeling, Supplement of Evaluation 12: Update of Key Reactions, JPL Publ, 00-3*, Jet Propul. Lab., Pasadena, Calif., 2000.

Stockwell, D. Z., M. A. Kritz, M. P. Chipperfield, and J. A. Pyle, Validation of an off-line three-dimensional chemical transport model using observed radon profiles, 2, model results, *J. Geophys. Res.*, *103*, 8433–8445, 1998.

Sudo, K., and M. Takahashi, Simulation of tropospheric ozone changes during 1997–1998 El Niño: Meteorological impact on tropospheric photochemistry, *Geophys. Res. Lett.*, *28*, 4091–4094, 2001.

Sudo, K., M. Takahashi, and H. Akimoto, CHASER: A global chemical model of the troposphere, 2, Model results and evaluation, *J. Geophys. Res.*, *107*, 10.1029/2001JD001114, in press, 2002.

Takemura, T., H. Okamoto, Y. Maruyama, A. Numaguti, A. Higurashi, and T. Nakajima, Global three-dimensional simulation of aerosol optical thickness distribution of various origins, *J. Geophys. Res.*, *105*, 17,853–17,873, 2000.

Takigawa, M., M. Takahashi, and H. Akiyoshi, Simulation of ozone and other chemical species using a center for climate system research/national institute for environmental studies atmospheric gcm with coupled stratospheric chemistry, *J. Geophys. Res.*, *104*, 14,003–14,018, 1999.

Talukdar, R. K., C. A. Longfellow, M. K. Gilles, and A. R. Ravishankara, Quantum yields of $O(^1D)$ in the photolysis of ozone between 289 and 329 nm as a function of temperature, *Geophys. Res. Lett.*, *25*, 143–146, 1998.

van Leer, B., Toward the ultimate conservative difference scheme, part IV, A new approach to numerical convection, *J. Comput. Phys.*, *23*, 276–299, 1977.

Van Pul, W. A. J., *The flux of ozone to a maize crop and the underlying soil during a growing season*, Ph.D. thesis, Wageningen Agric. Univ., Wageningen, Netherlands, 1992.

Velders, G. J. M., and C. Granier, Sensitivity of washout on HNO_3/NO_x ratio in atmospheric chemistry transport models, *J. Geophys. Res.*, *106*, 3125–3132, 2001.

Wang, Y., D. J. Jacob, and J. A. Logan, Global simulation of tropospheric O_3-NO_x-hydrocarbon chemistry, 1, Model formulation, *J. Geophys. Res.*, *103*, 10,713–10,725, 1998a.

Wang, Y., J. A. Logan, and D. J. Jacob, Global simulation of tropospheric O_3-NO_x-hydrocarbon chemistry, 2, Model evaluation and global ozone budget, *J. Geophys. Res.*, *103*, 10,727–10,755, 1998b.

Wang, Y., D. J. Jacob, and J. A. Logan, Global simulation of tropospheric O_3-NO_x-hydrocarbon chemistry, 3, Origin of tropospheric ozone and effects of nonmethane hydrocarbons, *J. Geophys. Res.*, *103*, 10,757–10,767, 1998c.

Wesely, M. L., Parameterization of surface resistance to gaseous dry deposition in regional-scale numerical models, *Atmos. Environ.*, *23*, 1293–1304, 1989.

Yienger, J. J., and H. Levy II, Empirical model of global soil-biogenic NO_x emissions, *J. Geophys. Res.*, *100*, 11,447–11,464, 1995.

H. Akimoto, Institute for Global Change Research, Yokohama Campus, 3173-25 Showa-machi, Kanazawa-ku, Yokohama, Kanagawa, 236-0001, Japan. (akimoto@frontier.esto.or.jp)

J. Kurokawa, Systems Department, Environmental Systems Business Division, Fujitsu FIP Corporation, Times 24 Bldg., 2-45, Aomi Koutou-ku, Tokyo, 135-73, Japan. (kurokawa@fip.co.jp)

K. Sudo and M. Takahashi, Center for Climate System Research, University of Tokyo, 4-6-1, Komaba, Meguro-ku, Tokyo, 153-8904, Japan. (kengo@ccsr.u-tokyo.ac.jp; masaaki@ccsr.u-tokyo.ac.jp)